Title
RELATION OP TOUGHNESS TO MICROSTRUCTURE IN SPHEROIDIZED STEEL

Author
Atherton, Charles Sheldon.

Publication Date
1971-03-01

UCRL-20540

RELATION OF TOUGHNESS TO MICROSTRUCTURE IN SPHEROIDIZED STEEL

Charles Sheldon Atherton
(M. S. Thesis)

March 1971

AEC Contract No. W-7405-eng-48

LAWRENCE RADIATION LABORATORY
UNIVERSITY of CALIFORNIA BERKELEY

UCRL-20540

DISCLAIMER

TABLE OF CONTENTS

RELATION OF TOUGHNESS TO MICROSTRUCTURE IN SPHEROIDIZED STEEL

Charles Sheldon Atherton

Inorganic Materials Research Division, Lawrence Radiation Laboratory
Department of Materials Science and Engineering, College of Engineering
University of California, Berkeley, California

Abstract

The tensile and fracture toughness properties of a 1070 steel spheroidized by warm rolling below the α-γ transformation temperature are compared with grain and particle size measurements. Carbide particles are located predominantly at grain boundaries. Mean grain and particle diameters are reduced to as small as 0.6μ and 0.2μ respectively. The room temperature yield strength is increased from 50 ksi for pearlite to 130 ksi. The room temperature fracture toughness is increased from 67 ksi-in$^{1/2}$ for pearlite to 106 ksi-in$^{1/2}$. Fine particles are found to produce greater toughness than coarser particles.

LIST OF SYMBOLS

K	stress intensity parameter describing the elastic stress field in the vicinity of the crack. The value of K at instability is referred to as the fracture toughness and has units of psi-in$^{1/2}$.
I	subscript denoting first or opening mode of fracture. Referred to as plane-strain condition.
C	subscript denoting critical value of a parameter.
B	specimen thickness, in.
a	crack length, in.
W	specimen width, in.
E	Young's modulus, psi.
P	applied load, lbs.
COD, ν	crack opening displacement, in.
σ_{YS}	yield stress, psi.
σ_{LYS}	lower yield stress, psi.
D,d	mean intercept grain diameter.

I. INTRODUCTION

Since the discovery that polished and etched metals display a wide variety of microstructures, much effort has been expended to correlate mechanical properties with these features. The application of chemistry, thermodynamics, and, more recently quantum mechanics[1] to metallic solutions has allowed considerable control over the constituents of an alloy and their distribution. Similarly, a great deal of progress has been made in understanding the mechanical properties associated with different constituent arrangements with the development of dislocation mechanics. The field of fracture mechanics has introduced yet another microstructurally sensitive material property, fracture toughness, with which this paper is primarily concerned.

The distribution of carbon in a plain carbon eutectoid steel can be varied from plate-like lamellar carbide or lenticular martensite to one of spheroidized carbide. While this transformation has previously been accomplished by lengthy annealing,* it has been found[4,5] that spheroidization can be accelerated by deformation below the α-γ transformation temperature. In addition, the carbide particle size can be controlled by the choice of deformation temperature as well as by subsequent annealing of the spheroidized structure.

---

*A fine spheroidized structure can also be obtained by deformation during the γ to α transformation,[2] or by cooling from deformed austenite.[3]

Using this technique, a commerical 1070 steel was warm rolled and annealed at several temperatures to yield specimens with different particle and grain sizes. The tensile and fracture properties of these structures were then evaluated and compared with grain and particle size measurements. In addition, scanning electron microscopic examinations were made of the fracture surfaces and the stress wave emission (SWE) technique was used to monitor elastic waves emitted by discontinuous crack growth prior to fracture.

II. EXPERIMENTAL PROCEDURE

A. Material Preparation

Commerical 1070 steel was received as a 2"X3"X36" bar with the following chemical composition: 0.77% C, 0.8% Mn, 0.2% Si, 0.04% Cu, 0.04% Cr, 0.01% Ni, 0.026% S, 0.013% P, 0.008% Mo. The bar was cut into 6" lengths, austenitized at 800°C for two hours and furnace cooled.

1. Mechanical Treatment

The pearlitic bars were reheated to temperatures of 500°C, 600°C or 700°C and rolled with pre-warmed rolls, reheating for five minutes between passes. The bars were air cooled after rolling and cut to sizes appropriate for tensile and fracture toughness specimens. Samples were taken for metallographic examination.

2. Heat Treatment

Prior to heat treatment of the actual test specimens, the samples for metallographic examination and microhardness tests were placed in argon filled quartz tubes and annealed at 500°C, 600°C or 700°C for various times. The results of tests on these preliminary samples were then used to select appropriate heat treatments for the tensile and fracture toughness specimens.

Tensile and fracture specimens were then enclosed together in stainless steel heat treatment bags to minimize exposure to air during annealing. The specimens were air cooled upon removal from the annealing furnace.

3. Machining

The tensile and fracture specimens were machined to the dimensions shown in Figs. 1 and 2. Fracture specimens were machined so that the fracture plane would be perpendicular to the rolling direction. Tensile specimens were machined with the tensile axis in the longitudinal director.

For tensile test specimens, bars rolled at 600° and 700°C (final thickness of 0.38") were cut longitudinally, so that tensile specimens were taken from the upper and lower halves of the rolled bar. However, the bars rolled at 500°C (thickness 0.46") were cut twice longitudinally so that the tensile specimens were taken from the upper face, lower face and center of the rolled bar.

B. Mechanical Testing

1. Tensile Tests

An Instron testing machine was used at a cross-head speed of .05 cm/min. Tests at -75°C were made by immersing the specimen in ethanol and dry ice. Tests at -20°C were performed by adding dry ice to the ethanol bath at intervals. The volume of ethanol was great enough to maintain the bath temperature to within ±1°C.

2. Fracture Toughness Tests

Fatigue cracks were introduced into the fracture toughness specimens by a Materials Testing System (MTS) machine using a sinusoidal cycle with load alternating between 50 and 1800 pounds, or a maximum stress intensity of 40 ksi-in$^{1/2}$, at a frequency of 6Hz. An average of 10,000 cycles were required to obtain the proper crack length of .063" (a/W = 0.50).

As the applied load was increased during testing, the change in displacement between two knife edges machined in the fracture specimen was measured by a crack opening displacement (COD) gauge described in reference 6. One fracture toughness sample was sacrificed to calibrate the compliance of the specimen geometry at known crack lengths. The calibration curve of Fig. 3 was obtained from the slope of load versus COD of the elastically loaded calibration sample at various ingrements of crack length extended by machining between tests. This calibration curve was used to calculate the effective crack length from the load versus COD curve of actual fracture tests. The criterion for selecting the point on the load versus COD curve from which the fracture toughness values were calculated was the point of maximum load, even though this might not correspond to the critical load and crack length in cases of failure by tearing (see Figs. 12, 14, and 15).

Most of the fracture toughness tests were conducted on an Instron testing machine since much sensitivity in recording stress wave activity was lost in filtering out the higher noise levels of the MTS. The cross-head speed was 0.20 cm/min., giving a rate of increase of stress intensity (10^6 psi-in$^{1/2}$/min) within the range recommended by the ASTM Standards.[7] The COD gauge output was used to drive the Instron recording chart.

Fracture tests of several specimens at room temperature and at -75°C along with data from Guest[8] indicated that the transition temperature for this alloy was about -20°C. In order to avoid having all the samples tear or cleave, the tests were conducted at the transition temperature. This also insured the maximum sensitivity of fracture toughness to microstructure.

Fracture toughness test temperatures of -75°C and -20°C were obtained by enclosing the specimen and grips in an insulating container and introducing nitrogen vapor through a perforated copper coil wound around the grips. A thermocouple within the notch of the specimen, along with a potentiometer-type temperature controller and a flow regulating system, brought the sample to the test temperature within about twenty minutes. The test was not begun until the thermocouple voltage was checked on a more sensitive, calibrated potentiometer. The apparatus is shown in Fig.4.

3. Stress Wave Emission Technique[13-15]

The elastic stress waves emitted by discontinuous crack growth prior to failure were recorded by the apparatus shown schematically in Fig. 5. The apparatus and test setup are illustrated in Fig. 6. The band pass filter was set for a low pass of 40 kHz and the high pass was varied from 5 to 25 kHz. The best results for tests on the instron were obtained at a high pass of 15 kHz. The total gain of the system was varied between 36,000 and 90,000.

C. Microscopy

1. Metallography

Metallographic samples were etched in nital and photographed at 2000X using oil emersion of a Zeiss metallograph. From one to four photomicrographs of specimens selected for quantitative microstructural analysis were enlarged two and a half times, and these enlargements were used for the analysis. All photomicrographs used in the quantitative analysis were transverse to the rolling direction. The mean intercept transverse grain diameter was determined from the ratio of the length of traverse across a microstructure to the number of grain boundaries intersected.

The apparent transverse particle size was found by dropping a cricular template on the photomicrograph at random, and measuring the apparent diameters of particles whose centers fell within the circle. To evaluate the number of particles per cubic millimeter and the volume fraction occupied by the carbides, the Saltvkov[9] method was used, the particles being divided into seven size groups.

2. Fractography

Immediately after fracture, of a specimen, a hot blower was directed on the fracture surface to remove ice which had condensed from the air. Fracture surfaces selected for electron microscopic examination were taped to prevent mechanical damage and contamination by extraneous particles, then cut from the fracture specimen by hand to avoid overheating or exposure to water. The fracture surfaces were cleaned ultrasonically while immersed in 200 proof ethanol, then stored in dessicators until examined in the scanning electron microscope.

III. EXPERIMENTAL RESULTS

A. Material Preparation

In order to obtain a fully spheroidized structure[4] the steel must be deformed to a true strain of 2.0. To obtain this heavy reduction and maintain thickness, it was necessary to rotate the bars 90° for several passes. Rolling under these conditions required up to 70 passes and eight hours at temperature.

At rolling temperatures of 600 and 700°C, the pearlitic bars (2"×3" cross section) could be deformed to the required strain (0.40"×2.0" cross section) without excess difficulty. However, at the 500°C rolling temperature, edge cracking began and become so severe at higher strains that rolling was terminated at a true strain of 1.8. This resulted in the incompletely spheroidized structure shown in Fig. 11(a).

B. Mechanical Behavior

1. Tensile Behavior

The results of tensile tests are listed in Table I and plotted versus anneal time in Fig. 7. Most tests were conducted at room temperature. Testing at -75°C raised the yield and tensile strengths an average of 10 and 15 ksi, respectively. The only samples which did not exhibit yield point phenomena were the pearlitic structure and the incompletely spheroidized specimens taken from the outer faces of the bar rolled at 500°C. However, a Luder's strain appeared for the specimen taken from the central portion of the 500°C rolled bar, as well as in all those specimens annealed after rolling. Microhardness tests and examination of the microstructure

across the thickness of specimen rolled at 500°C failed to show any variation with thickness.

The yield stress was determined using either the load during the Luder's strain or, where no yield phenomena occurred, the load at 0.2% offset.

2. Fracture Toughness Behavior

The results of fracture toughness tests are listed in Table II.

The most striking feature of the test is the wide variation in fracture surface appearance, shown in Fig. 8. Whereas the pearlitic structure cleaved at both -75°C and room temperature, the fracture surface appearance of the spheroidized samples varied from a heavily serrated form of ductile rupture to predominantly cleavage rupture. A comparison of the fracture surfaces of Fig. 8 with the toughness data of Table II indicates that this serrated mode of failure enhances toughness. In case of failure by a mixed mode of cleavage and serrated ductile rupture the later mode appears in the central portion of the fracture surface. The serration effect is reduced at longer annealing times.

3. Stress Wave Emission Results

Several examples of stress wave emissions are shown in Figs. 10,12, 14-16 and 18 with the regions of the load versus COD curve from which they are taken marked on the curve. Stress wave emission from the samples of Figs. 10 and 12 were recorded at a high pass of 15 kHz and a gain of 36,000 while the stress waves shown in the remaining figures were recorded at a high pass of 5 kHz and a gain of 90,000. The number of stress waves counted prior to maximum load for several specimens are listed in Table III.

C. Microscopy

1. Metallography

The low resolution of the optical microscope at 2000 made examination of the fine particle sizes of samples rolled at 500°C difficult (see Fig. 11). For this reason, and since the microstructures were not completely spheroidized, particle size measurements were not attempted on samples rolled at 500°C.

It can be seen from several of the photomicrographs that carbides are located predominantly at grain boundaries.

The results of quantitative microscopic analysis on selected samples are shown in Table IV. Figure 19 shows the distribution of apparent transverse particle sizes for the two samples most widely separated in particle density of those analyzed.

2. Fractography

The most prominent fractographic feature of the samples of this investigation is the formation of longitudinal "chimneys" during ductile fracture. From Figs. 13 and 20 it appears that these chimney coalesce parallel to the crack growth direction to nucleate the macroscopic serrations. Traces of these chimneys are observed on the faces of the serrations.

IV. DISCUSSION

A. Material Preparation

Sherby obtained a yield strength of 130 ksi with 5 per cent elongation by rolling a eutectoid steel at approximately 500°C to a true strain of 2.0. This was accomplished in 14 passes with five minutes between each pass at a furnace temperature of 600°C. In addition, he found the yield strength to increase slightly and the ductility to triple upon annealing at 500°C for 6000 minutes. In the present investigation the elongation increased upon annealing but as can be seen in Fig. 7 no secondary hardening was observed. This could be a result of the considerable difference in time at temperature during rolling as well as the smaller strain of 1.8 obtained.

Sherby has suggested that edge cracking might be avoided by maintaining a rectangular cross-section during rolling.

B. Mechanical Behavior

1. Tensile Tests

The plot of yield strength versus the inverse square root of the mean intercept grain diameter of Fig. 21 agrees with the data of Petch for a .11% C steel. This would be expected as long as carbides remain at the grain boundaries. The equation of this line follows the Hall-Petch relation:

$$\sigma_{LYS} = \sigma_0 + Cd^{-1/2}$$

where σ = 9,000 psi, C = 94,000 psi-$in^{1/2}$ and d is the grain diameter in inches.

The lack of a Luder's strain in the specimens rolled at 500°C and machined from the bar surface, and its appearance in the specimen taken from the center of the bar, imply that spheroidization was more complete at the center. However, the tensile strengths of these specimens adjusted to room temperature show no significant difference, which accounts for the uniform Vicker's hardness observer across the thickness of the bar. The fact that the yield strength and fracture toughness of these specimens correlates well with the remaining data suggests that the effect of incomplete spheroidization was minimal.

The specimens rolled at 500°C and annealed for various times at 500°C, in agreement with Sherby's data, showed no strain hardening but necked without exceeding the lower yield stress.

2. Fracture Toughness Tests

For strength levels of (K_{IC}/σ_{LYS}) for materials similar to those used in this investigation, Brown and Srawley[6] found that the specimen thickness, B, required for a valid plane strain fracture toughness tests was $B \geq 2.5\ (K_{IC}/\sigma_{YS})^2$. Wessel[10] found that for materials of the same yield strength as those presented here, a less stringent requirement of $B \geq (K_{IC}/\sigma_{YS})^2$ gave consistent values of K_{IC}. Both of these criteria are shown in the plot of K/σ_{LYS} vs. σ_{LYS} in Fig. 22, and it can be seen that only a few fracture toughness values at -75°C satisfy Wessel's criterion for K_{IC}.

In Fig. 22 the samples are divided according to their particle densities. Since the yield strength depends only on the grain size for these materials, this plot shows the dependence of fracture toughness on particle size. It can be seen that smaller particles give a higher

toughness than larger ones, especially at the -20°C test temperature. Again, the ductile serration mode of failure predominates in these tougher specimens.

Longitudinal cracks similar to those observed in this investigation were observed by Beachem et al.[11] in fracture tests of A302-B pressure vessel steel, and were attributed to stringer inclusions. Liu and Gurland[12] observed the formation of cracks parallel to the tensile axis in the necked region of spheroidized plain carbon steel tensile specimens. These were nucleated from interfacial cracks at grain boundary carbides.

3. Stress Wave Emission

Not enough stress wave data was analyzed to show clear trends with particle and grain size. In addition, the various high band passes used in filtering extraneous noise and the different gains used to amplify the accelerometer signal made stress wave comparisons of different samples and test temperatures difficult. However the data does show approximately an order of magnitude increase in stress wave activity at test temperatures of -75°C above that at -20°C.

C. Microscopy

1. Metallography

Although the carbides in most samples were located at the grain boundaries, there was a tendency for more particles to be located within grains in samples rolled at 500 or 600°C and annealed at 600 or 700°C. Apparently the smaller particles formed at lower rolling temperatures are unable to pin grain boundaries at the higher annealing temperatures. Unfortunately, the fraction of particles located at grain boundaries was

not determined in the quantitative microstructural analysis. This observation does suggest a means of separating the effects of particles located within grains and those located at grain boundaries.

V. CONCLUSIONS

1. Spheroidization of a plain carbon eutectoid steel by warm rolling produces a grain size of almost half a micron and a mean particle size of less than 0.2 microns.

2. The yield strength is increased from 50 ksi for pearlite to 130 ksi for a rolling temperature of 500°C.

3. Yield strength versus the inverse square root of mean intercept grain diameter follows a Hall-Petch relationship.

4. The room temperature fracture toughness increases from 67 ksi-in$^{1/2}$ for the pearlitic structure to 106 ksi-in$^{1/2}$ for the spheroidized structure formed by rolling at 500°C. The fracture toughness at -75°C is increased from 41 ksi-in$^{1/2}$ for the pearlitic structure to 88 ksi-in$^{1/2}$ for the spheroidized structure produced by rolling at 600°C.

5. Fracture toughness is higher for small grain boundary carbides than for large grain boundary carbides. This effect is less pronounced at -75°C than at -20°C.

ACKNOWLEDGEMENTS

The author would like to express his appreciation to Dr. Victor F. Zackay and especially to Dr. William W. Gerberich for their advice and support.

The assistance of the staff of the Inorganic Materials Research Division of the Lawrence Radiation Laboratory is gratefully acknowledged, especially John Holthius (fabrication), J. A. Patenaude (machining), Lee Johnson (metallography), Don Krieger (testing), and Jane Ball (preparation of manuscript).

This work was done under the auspices of the U.S. Atomic Energy Commission through the Inorganic Materials Research Division of the Lawrence Radiation Laboratory.

REFERENCES

1. Leo Brewer, "Predictions of High Temperature Metallic Phase Diagrams", in High Strength Materials, Victor F. Zackay, ed., John Wiley & Sons, (1965) p. 12.

2. J. J. Irani, "Isoforming - A Technique of Deformation During Isothermal Transformation to Pearlite," JISI, April 1968, p. 363.

3. J. L. Uvira, D. B. Clay and J. D. Embury, "Controlled Deformation and Cooling of a Eutectoid Carbon Steel," Metals Engin. Quarterly, February 1970, p. 35.

4. O. D. Sherby, M. J. Harrigan, L. Chamagne and C. Sauve, "Development of Fine Spheroidized Structures by Warm Rolling of High Carbon Steels," Trans. ASM, 62, 1969, p. 575.

5. E. A. Chojnowski and W. J. McG. Tegert, "Accelerated Spheroidization of Pearlite," Metal Science Journal, 2, (1968), p. 14.

6. W. F. Brown, Jr., and J. E. Srawley, "Plane Strain Crack Toughness Testing of High Strength Metallic Materials," ASTM STP No. 410, 1967.

7. "Proposed Method of Test for Plane-Strain Fracture Toughness of Metallic Materials," ASTM Standards, 31, May 1969, pp. 1099-1114.

8. Peter J. Guest, "The Micromechanics of Fracture of Pearlitic Structural Steels," University of California, Lawrence Radiation Laboratory, UCRL-19106, December 1969.

9. Ervin E. Underwood, "Particle Size Distribution," in Quantitative Microscopy, Robert T. Delloff and Frederick N. Rhines, eds., McGraw Hill (1968) p. 167.

10. E. T. Wessel, "State of The Art of the WOL Specimens for K_{IC} Fracture Toughness Testing," Engin. Fracture Mech., 1, 77-103 (1968).

11. C. D. Beachem, T. C. Lupton and B. F. Brown, "A New Technique for Examining Microscopic Fracture Processes at Crack Tips," Met. Trans. 2, January 1971, p. 141.

12. C. T. Liu and J. Gurland, "The Fracture Behavior of Spheroidized Carbon Steels," Trans. ASM, 61, 1968, p. 156.

13. W. W. Gerberich and C. E. Hartbower, "Some Observations on Stress Wave Emission as a Measure of Crack Growth," Int. J. Fracture Mech. 3, (3), 185-92 (1967).

14. C. E. Hartbower, W. W. Gerberich and P. P. Cummings, "Monitoring Subcritical Crack Growth by Detection of Elastic Stress Waves," Welding J., Research Supplement, January 1968.

15. C. E. Hartbower, W. W. Gerberich, and H. Liebowitz, "Investigation of Crack-growth Stress-wave Relationships," Engi. Fracture Mech. 1, 291-308 (1968).

16. American Society for Testing and Materials, "Tension Testing of Metallic Materials," ASTM Standards, 31, 1967 p. 705.

TABLE I. Tensile test data

Sample	Processing: Rolling	Processing: Anneal	Anneal	Test Temp.	Lower Yield Stress (ksi)	Tensile Strength (ksi)	Elongation (%)	Reduction in area (%)	Luder's Strain (%)
0-1	---	---	---	R.T.	52.7*	111	9.05	19.7	0
0-2	---	---	---	R.T.	52.6*	115	14.4	18.8	0
0-3	---	---	---	R.T.	53.4*	114	12.7	18.9	0
0-4	---	---	---	R.T.	48.0*	114	13.1	19.4	0
0-5	---	---	---	R.T.	50.3*	112	12.7	20.0	0
5000-1	500	---	---	R.T	77.1*	140	5.74	24.4	0
5000-2	500	---	---	-75	85.0*	153	6.19	23.4	0
5000-3	500	---	---	-20	134†	144	4.12	27.2	1.1
5533	500	500	3	R.T.	114†	121	11.3	33.1	2.8
5563	500	500	6	R.T.	111	111	7.03	37.1	4.5‡
5514	500	500	10	R.T.	110	110	10.1	34.9	8.3‡
5632	500	600	0.3	R.T.	99.4†	107	15.9	38.7	4.1
5613	500	600	1	R.T.	85.6†	97.7	21.4	42.9	3.5
5633	500	600	3	R.T.	82.4	90.8	24.7	47.9	5.5
5663	500	600	6	R.T.	75.0	82.6	19.5	52.7	6.0
5614	500	600	10	R.T.	69.2	78.0	20.7	58.2	5.8
5713	500	700	1	R.T.	63.6	79.0	28.1	60.6	3.4
6000-1	600	---	---	R.T.	96.2	104	21.1	48.3	3.0
6000-2	600	---	---	-75	108	123	18.4	22.1	0

*yield stress determined at 0.2% offset. No yield point.

†specimens cut from center of bar rolled at 500°C. These show yield point phenomena.

‡specimens necked during Luder's strain. Luder's strain measured to onset of necking.

TABLE I. Tensile test data (continued)

Sample	Processing Rolling	Anneal	Anneal	Test Temp.	Lower Yield Stress (ksi)	Tensile Strength (ksi)	Elongation (%)	Reduction in area (%)	Luder's Strain (%)
6613-1	600	600	1	R.T.	86.0	95.0	25.2	51.5	4.5
6613-2	600	600	1	R.T.	84.3	94.2	24.5	52.5	3.8
6633-1	600	600	3	R.T.	80.3	89.8	23.8	59.5	4.8
6633-2	600	600	3	R.T.	81.6	90.4	22.0	61.5	4.8
6614-1	600	600	10	R.T.	71.7	81.8	28.5	56.1	4.6
6614-2	600	600	10	R.T.	70.2	80.2	27.8	56.8	5.0
6713-1	600	700	1	R.T.	65.2	77.4	33.3	62.2	4.3
6713-2	600	700	1	R.T.	63.9	77.8	30.2	62.0	3.7
6763-1	600	700	6	R.T.	60.4	77.3	23.3	62.6	3.4
6763-2	600	700	6	R.T.	60.0	74.4	33.4	61.7	3.4
7000-1	700	---	---	R.T.	70.3	82.5	23.5	59.0	1.5
7000-2	700	---	---	-20	72.8	89.2	20.6	42.5	1.8
7000-3	700	---	---	-75	85.8	103	27.5	33.6	2.7
7000-4	700	---	---	-75	82.8	100	29.0	54.2	2.3
7623-1	700	600	2	R.T.	65.9	82.0	26.7	59.0	2.6
7623-2	700	600	2	R.T.	66.9	82.2	24.3	62.8	2.3
7614-1	700	600	10	R.T.	64.5	80.4	29.5	58.5	2.5
7614-2	700	600	10	R.T.	63.8	80.5	28.0	64.0	2.5
7713-1	700	700	1	R.T.	61.2	77.7	26.6	62.5	2.9
7713-2	700	700	1	R.T.	60.2	77.0	32.2	61.1	3.0
7714-1	700	700	10	R.T.	54.5	71.6	29.4	61.2	2.8
7714-2	700	700	10	R.T.	54.2	71.8	31.5	62.3	2.4

TABLE II. Fracture toughness data

Sample Number	PROCESSING Rolling Temp. (°C)	Anneal Temp. (°C)	Anneal Time ($min \times 10^{-3}$)	FATIGUE CRACKING Fatigue Load Range (lbs.)	Fatigue Cycles	Initial* Crack Length (a/w)	TESTING Test Temp. (°C)	Fracture+ Toughness ksi-in$^{1/2}$	Criterion‡ for K	Fracture Surface Appearance
0	---	---	---	50-1800	10,300	.52	-75	40.8	CCL	cleavage
0X	---	---	---	50-1800	10,000	.47	R.T.	76.0[a]	CCL	cleavage
5000	500	---	---	50-1800	3,800	.53	R.T.	106	ML	ductile
5000X	500	---	---	50-1800	3,000	.51	-20	105	ML	ductile
5533	500	500	3	50-1800	6,100	.54	-20	132	ML	ductile
5563	500	500	6	50-1800	11,500	.54	-20	111[b]	ML	ductile
5514	500	500	10	50-1800	8,100	.52	-20	134	ML	ductile
5632	500	600	0.3	50-1800	9,100	.52	-75	48.7†	CCL	cleavage
5613	500	600	1	50-1800	14,000	.50	-75	49.7†	CCL	cleavage
5633	500	600	3	50-1800	12,300	.52	-75	54.4†	CCL	cleavage
5663	500	600	6	50-1800	13,300	.50	-75	56.7	CCL	cleavage
5614	500	600	10	50-1800	11,100	.53	-20	124	ML	ductile
5713	500	700	1	50-1800 50-2100	15,000 20,000	(.49) .50	-20	99.4[c]	ML	cleavage
6000	600	---	---	50-1800	7,700	.51	-20	160	ML	ductile
6000X	600	---	---	50-1800	10,000	.49	-75	87.7Δ	ML	mixed

*Taken from the initial slope of the load vs. COD curves

+Unless noted otherwise, fracture toughness is a K_C value.

†Satisfies Wessel's criterion for K_{IC}; $(K_{IC}/\sigma_{YS})^2$ B, where B is the specimen thickness.

ΔThis specimen displayed two pop-ins corresponding to K_{IC} values of 41.8 and 48.1 ksi-in$^{1/2}$ (see Fig. 14).

‡CCL; LOAD at critical crack length. ML; maximum load.

a. Specimen pulled accidentally before test to a COD of .217"
b. Instron on PACE, toughness values appears low.
c. Fatigue load too large. Plastic zone visible about fatigue crack tip.

TABLE II. Fracture toughness data (continued)

Sample Number	PROCESSING Rolling Temp. (°C)	Anneal Temp. (°C)	Anneal Time ($min \times 10^{-3}$)	FATIGUE CRACKING Fatigue Load Range (lbs.)	Fatigue Cycles	Initial* Crack Length (a/w)	TESTING Test Temp. (°C)	Fracture+ Toughness ksi-$in^{1/2}$	Criterion‡ for K	Fracture Surface Appearance
6613	600	600	1	50,1800	10,000	.50	-20	121	CCL	mixed
6613X	600	600	1	50,1800	7,500	.52	-20	103	CCL	mixed
6633	600	600	3	50,1800	11,300	.49	-20	70.0	CCL	mixed
6633X	600	600	3	50,1800	12,400	.50	-75	50.1†	CCL	cleavage
6614	600	600	10	50-1800	12,200	.53	-20	135	CCL	mixed
6614X	600	600	10	50-1800	10,800	.50	-75	53.7	CCL	cleavage
6713	600	700	1	50-1800	10,700	.50	-20	187[d]	CCL	cleavage
6713X	600	700	1	50-1800	12,400	.50	-20	98.3	CCL	cleavage
6763	600	700	6	50-1800	9,600	.50	-20	96.0	CCL	cleavage
6763X	600	700	6	50-1800	13,000	.53	-20	110	CCL	cleavage
7000	700	---	---	150-1500 150-1800	10,400 10,400	.54	-20	63.7	CCL	mixed
7000X	700	---	---	50-1800 150-2100	10,000 1,000	.55	-20	140[e]	CCL	mixed
7623	700	600	2	50-1800	10,000	.51	-20	94.7	CCL	cleavage
7623X	700	600	2	50-1800	10,000	.54	-20	116	CCL	cleavage
7614	700	600	10	50-1800	10,000	.54	-20	112	CCL	cleavage
7614X	700	600	10	50-1800	7,900	.51	-20	128	CCL	cleavage
7713	700	700	1	70-1800	10,000	.52	-20	107	CCL	cleavage
7713X	700	700	1	50-1800	10,000	.50	-20	92.4	CCL	cleavage
7714	700	700	10	50-1800	9,100	.50	R.T.	196[f]	ML	ductile
7714X	700	700	10	50-1800	10,000	.52	-75	48.8	CCL	cleavage

d. Too large a preload put visible plastic zone about crack tip before test.
e. Fatigue load too large.
f. Pulled accidentally before test to a COD of .270".

TABLE III. Stress wave emission data

Specimen Number	PROCESSING Rolling Temp. (°C)	Anneal Temp. (°C)	Anneal Time (Min X10-3)	TEST CONDITIONS Test Temp. (°C)	Total‡ Gain (X10-3)	Band Pass Filter Low Pass (kHz)	Band Pass Filter High Pass (kHz)	Number of Stress Waves A Emitted
0	---	---	---	-75	36	40	15	216
5000	500	---	---	-20	36	40	15	222
5514	500	500	10	-20	36	40	15	63
5632	500	600	0.3	-75	36	40	15	146
5663	500	600	6	-75	36	40	10	431
5614	500	600	10	-20	90	40	5	19
6000	600	---	---	-20	90	40	5	62
6000X	600	---	---	-75	90	40	5	400†
6633	600	600	3	-20	90	40	5	38
6633X	600	600	3	-75	90	40	5	430
6614	600	600	10	-20	90	40	5	18
6614X	600	600	10	-75	90	40	5	374

*Stress waves were counted up to maximum load in the cases where failure occurred by tearing.

‡This is the factor by which the accelerometer output was amplified.

†The stress wave detection system was saturated by a large crack jumps, from COD 0.10" to 0.14". An appropriate number was added to the actual stress wave count of 338, using the stress wave activity immediately before and after the saturation occurred.

TABLE IV. Quantitative microstructural analysis

Sample Number	PROCESSING: Rolling Temp. (°C)	PROCESSING: Anneal Temp. (°C)	PROCESSING: Anneal Time (min$\times 10^{-3}$)	GRAIN SIZE ANALYSIS: Number of Grain Boundaries Intersected	GRAIN SIZE ANALYSIS: Length of Traverse (μ)	GRAIN SIZE ANALYSIS: Mean In Intercept Grain Diameter (μ)	PARTICLE SIZE ANALYSIS: Number of Particles Measured	PARTICLE SIZE ANALYSIS: Calculated† Volume Fraction of Fe_2C	PARTICLE SIZE ANALYSIS: †Number of particles/min^3 ($\times 10^{-6}$)
0	---	---	---	55	925	18.5*	Apparent Interlamellar Spacing ~1μ		
5000	500	---	---	360	231	.642	---	----	---
5514	500	500	10	553	457	.827	---	---	---
5614	500	600	10	373	673	1.80	204	.10	540
6000	600	---	---	398	446	1.12	296	.10	2400
6613	600	600	1	280	436	1.56	258	.13	950
6633	600	600	3	400	681	1.70	231	.10	810
6614	600	600	10	393	684	1.74	239	.10	660
6763	600	700	6	177	693	3.91	175	.11	170
7000	700	---	---	237	462	1.95	172	.11	740
7713	700	700	1	211	462	2.19	255	.09	250

*Mean intercept diameter of pearlite colonies.

†The volume fraction of Fe_3C and the number of particles/min^3 were determined by Salvkov's[9] method with the particles divided into seven size groups. The volume fraction of Fe_3C from the Fe-C phase diagram is 0.12.

Fig.15. (A) the load versus crack opening displacement, (B) the stress wave emission and (C) the fracture surface of a specimen rolled at 600°C without annealing and tested at -20°C.

Fig.16. (A) the load versus crack opening displacement curve, (B) the stress wave emission and (C) the fracture surface of a specimen rolled at 600°C, annealed at 600°C for 3000 minutes and tested at -20°C.

Fig.17. (A) the microstructure, and (B) the fracture surface at the fatigue-transgranular fracture transition of the sample of Fig. 18. The arrow shows the general direction of the crack propagation.

Fig.18. (A) the load versus crack opening displacement curve, (B) thre stress wave emission and (C) the fracture surface of a specimen rolled at 600°C, annealed at 600°C for 3000 minutes and tested at -75°C.

Fig.19. The apparent transverse particle size distribution of the specimens with the most widely separated particle densities of those analyzed. The upper distribution was for a specimen rolled at 600°C without annealing and the second is for a specimen rolled at 600°C and annealed at 700°C for 6000 minutes. The particle densities were obtained by the method of Saltykov[9], with the particles divided into seven size groups.

Fig.20. (A) the region of slow crack growth between fatigue and brittle fracture regions showing coalesced "chimneys" (B)a closer view of a serration surface showing what might be particle fragments on the wall of the "chimney".

Fig.21. The room temperature yield stress versus mean intercept grain diameter to -1/2. The key for identifying points is shown in Fig. 7.

Fig.22. K/σ_{LYS} versus σ_{LYS} for two classes of particle density and two test temperatures.

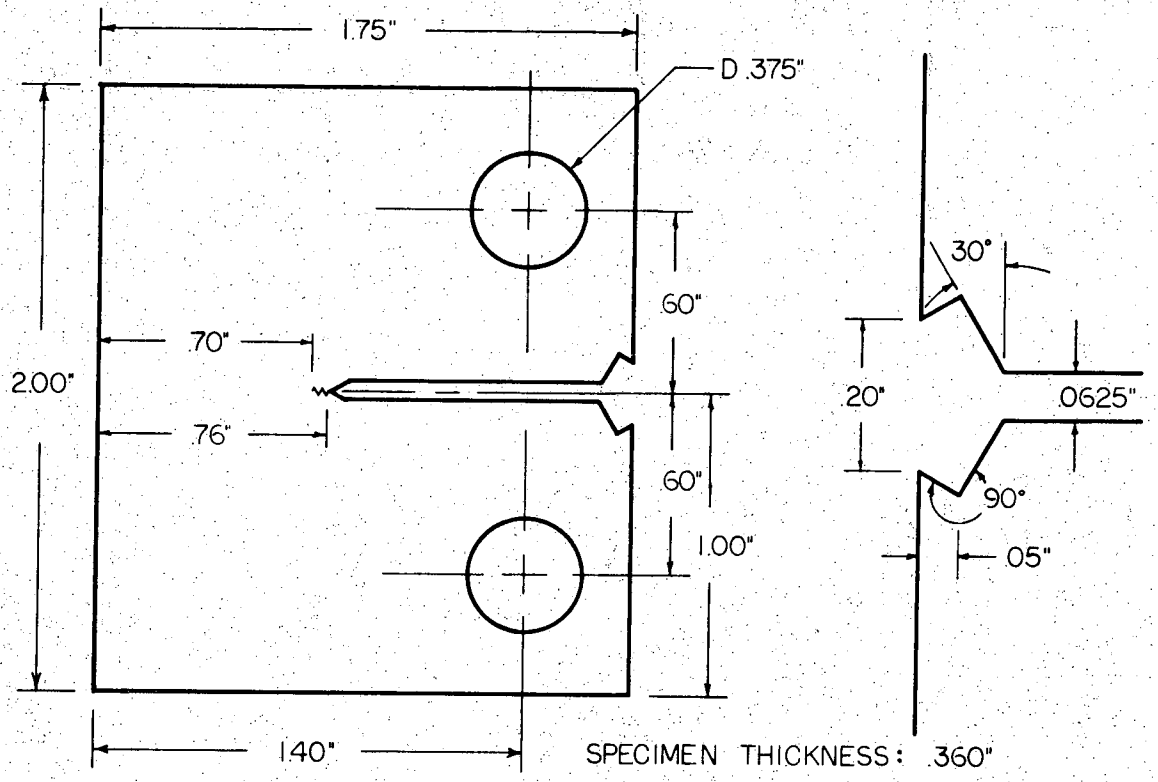
1.75"
D .375"
2.00"
.70"
.76"
.60"
.60"
1.00"
1.40"
30°
.20"
.0625"
90°
.05"
SPECIMEN THICKNESS: .360"
XBL713-6582

Figure 1

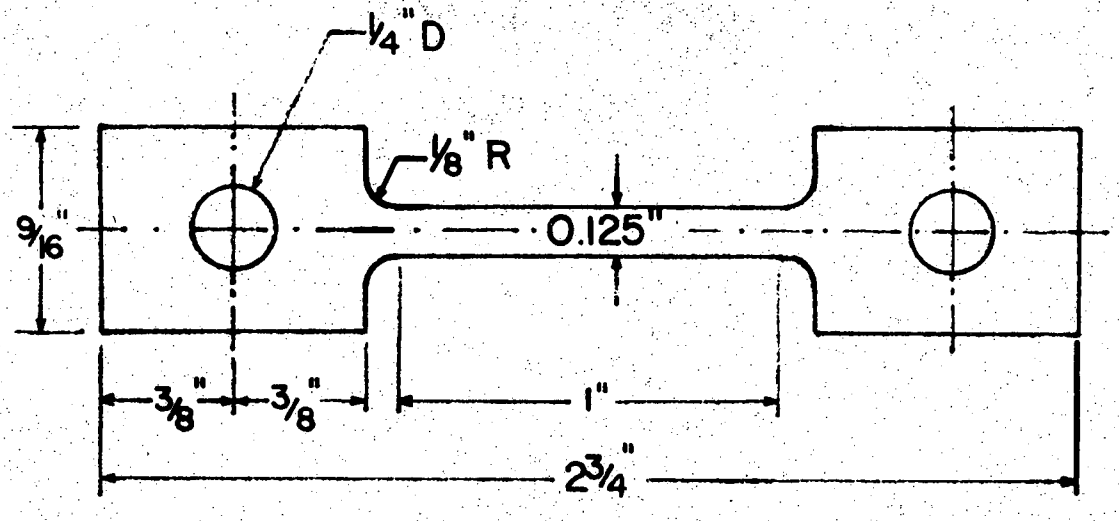

TENSILE SPECIMEN

SCALE: 2:1

XBL 698-1155

Figure 2

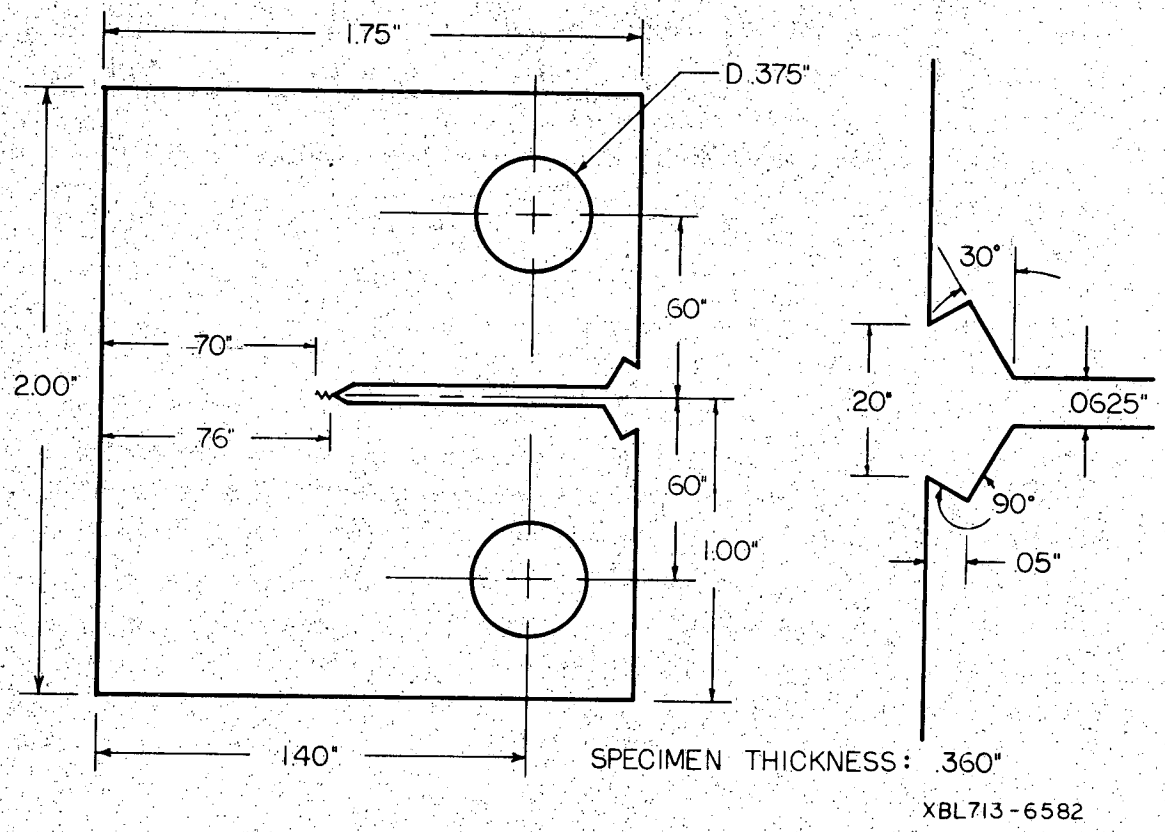
1.75"
D .375"
2.00"
.70"
.76"
.60"
.60"
1.00"
1.40"
30°
.20"
.0625"
90°
.05"
SPECIMEN THICKNESS: .360"
XBL713-6582

Figure 1

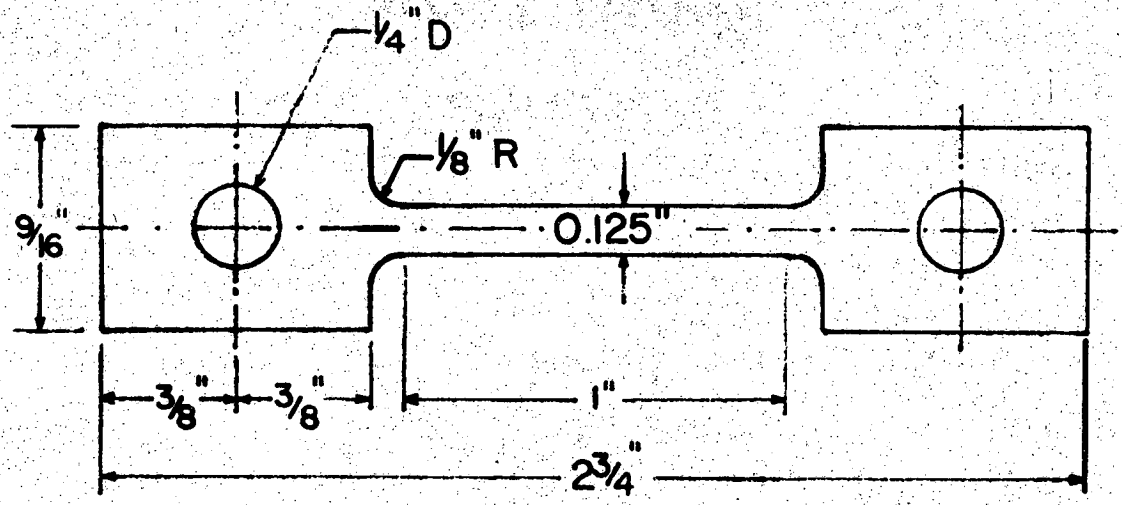

TENSILE SPECIMEN

SCALE: 2:1

XBL 698-1155

Figure 2

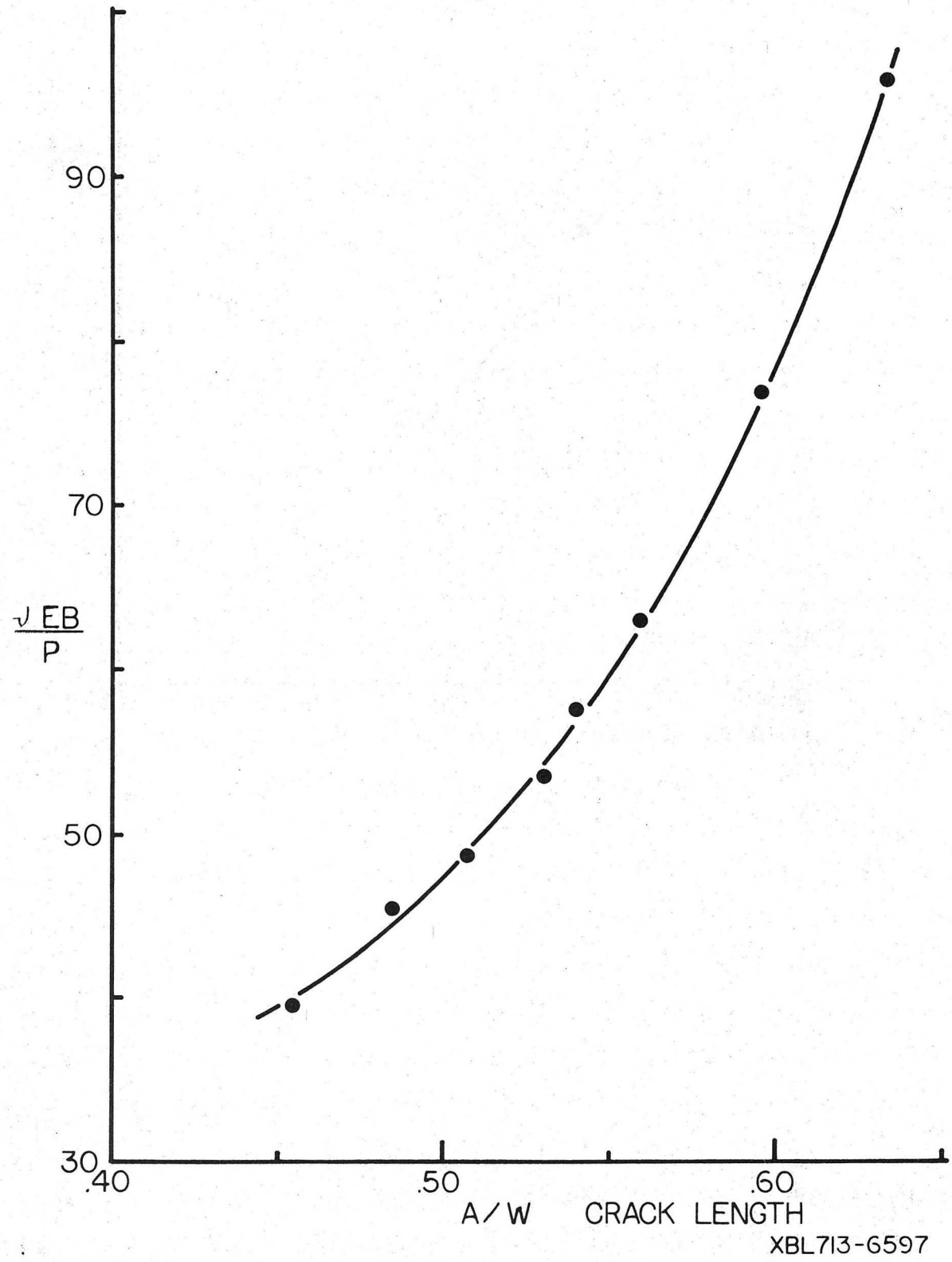

Figure 3

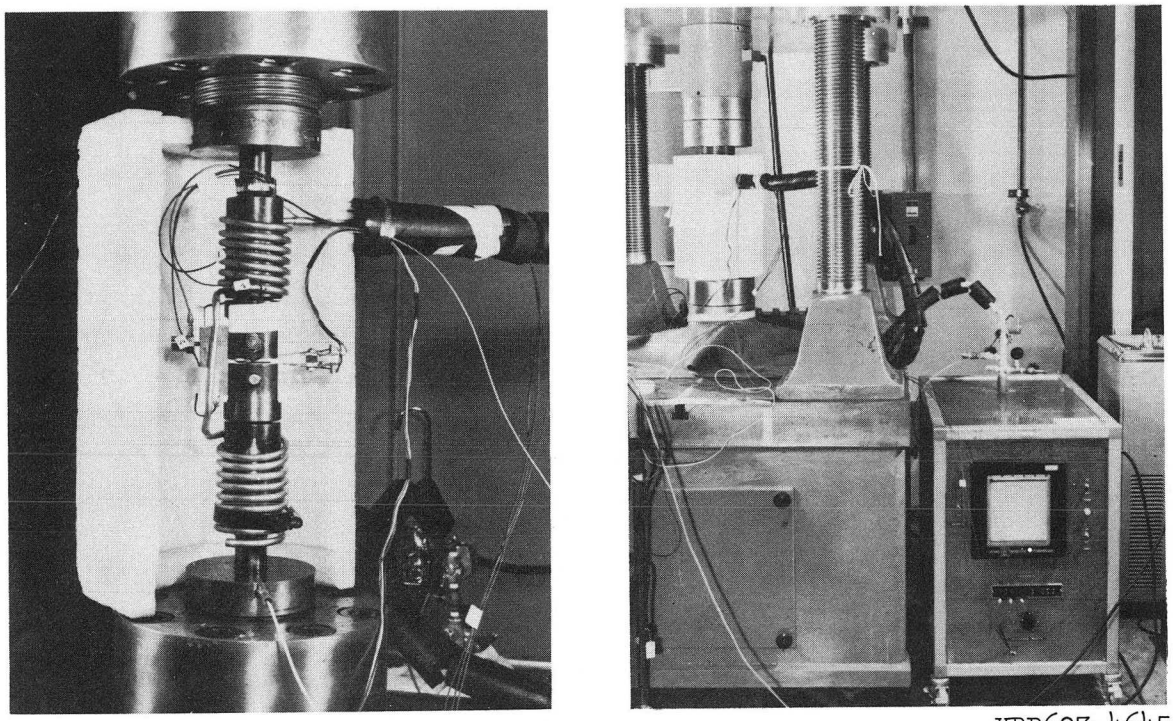

XBB697-4645

Figure 4

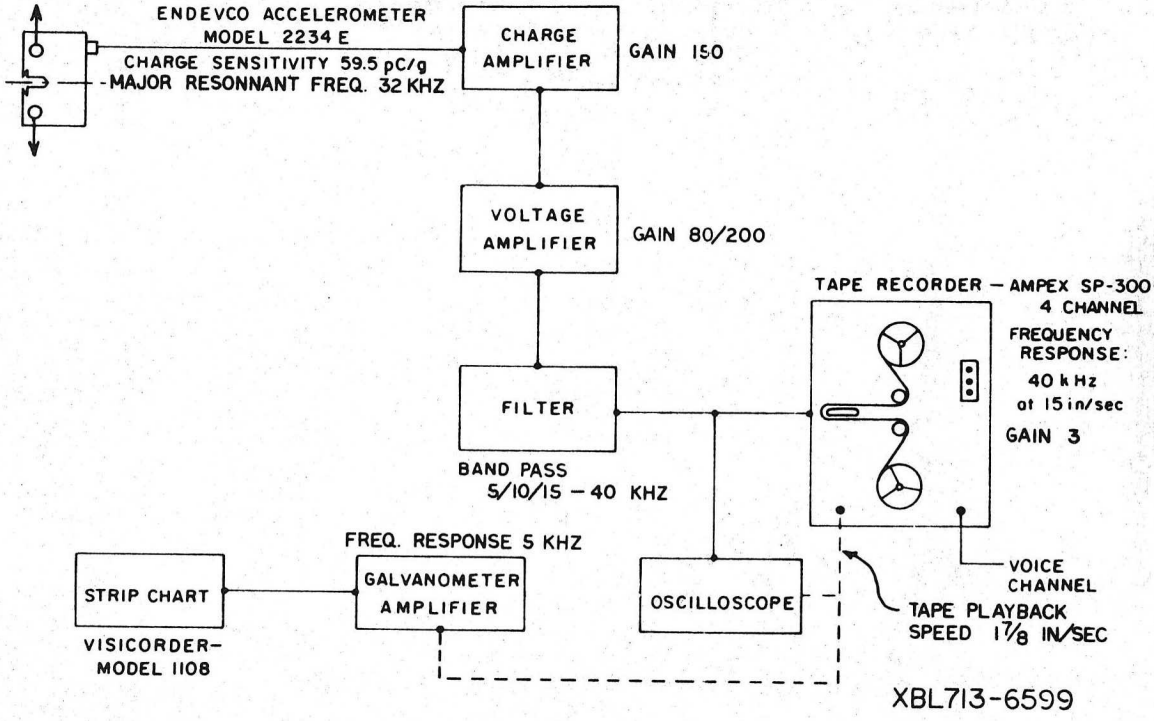
ENDEVCO ACCELEROMETER
MODEL 2234 E
CHARGE SENSITIVITY 59.5 pC/g
MAJOR RESONNANT FREQ. 32 KHZ
CHARGE AMPLIFIER
GAIN 150
VOLTAGE AMPLIFIER
GAIN 80/200
FILTER
BAND PASS
5/10/15 – 40 KHZ
TAPE RECORDER – AMPEX SP-300
4 CHANNEL
FREQUENCY RESPONSE:
40 k Hz
at 15 in/sec
GAIN 3
FREQ. RESPONSE 5 KHZ
STRIP CHART
VISICORDER–
MODEL 1108
GALVANOMETER AMPLIFIER
OSCILLOSCOPE
VOICE CHANNEL
TAPE PLAYBACK
SPEED 1 7/8 IN/SEC
XBL713-6599

Figure 5

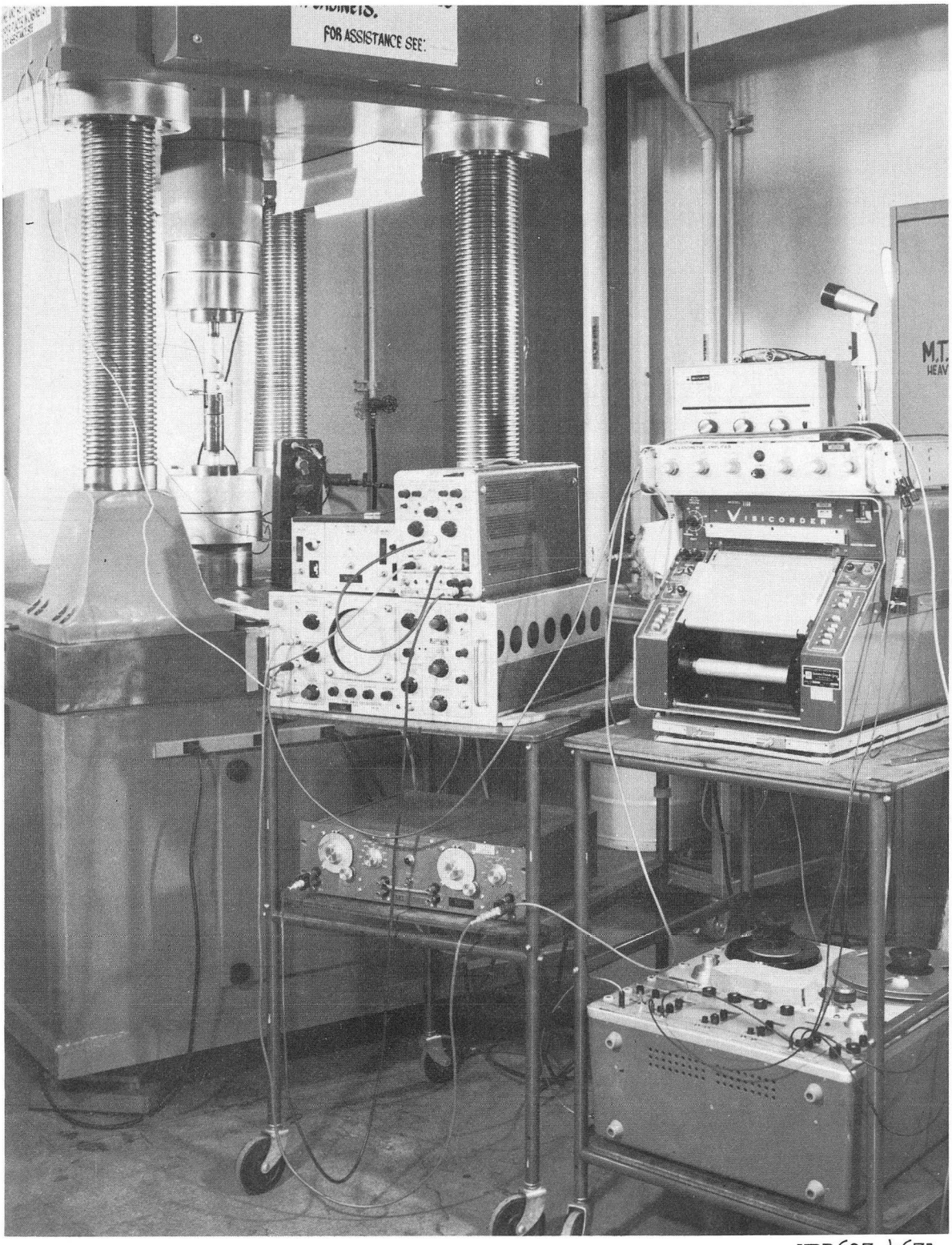

XBB697-4671

Figure 6

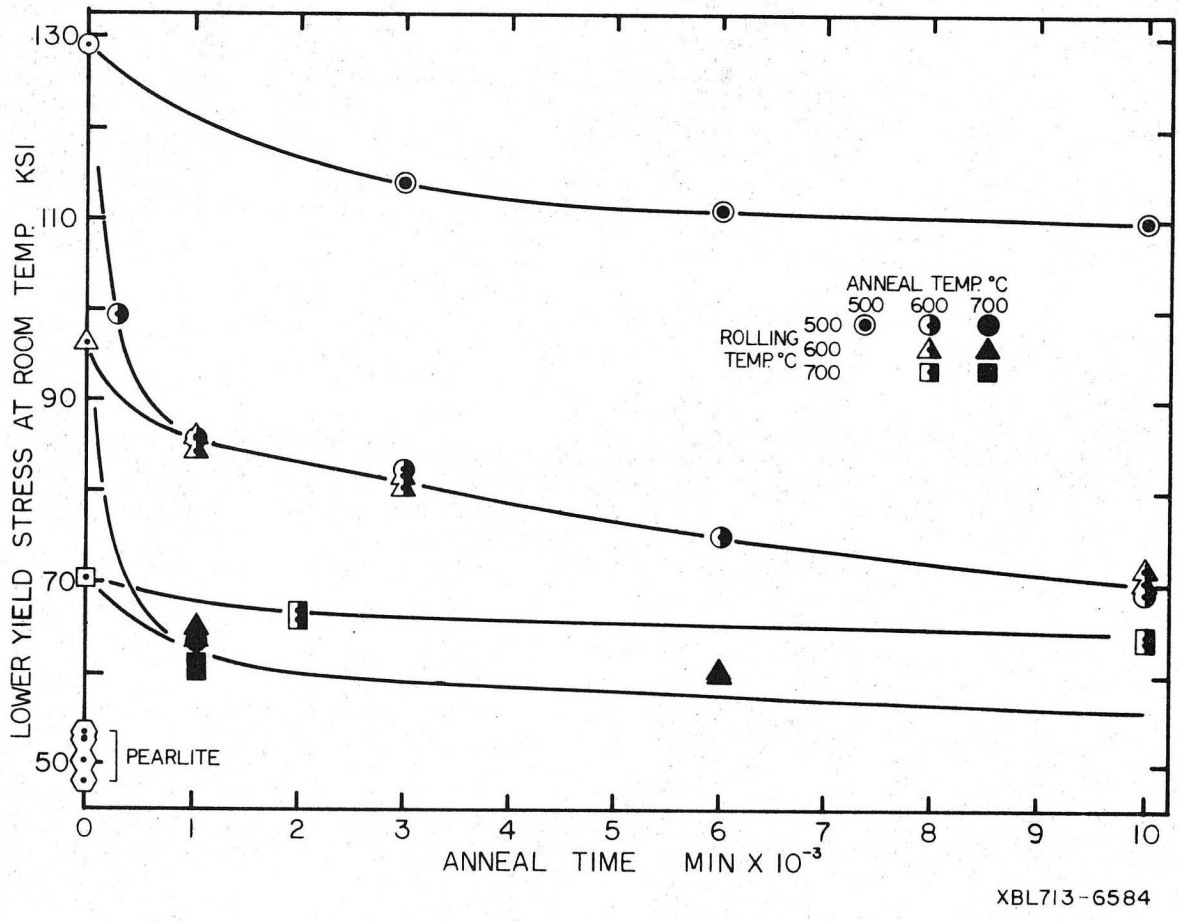
LOWER YIELD STRESS AT ROOM TEMP. KSI
130
110
90
70
50
PEARLITE
ANNEAL TEMP °C
500 600 700
ROLLING TEMP °C
500
600
700
0 1 2 3 4 5 6 7 8 9 10
ANNEAL TIME MIN X 10⁻³
XBL713-6584

Figure 7

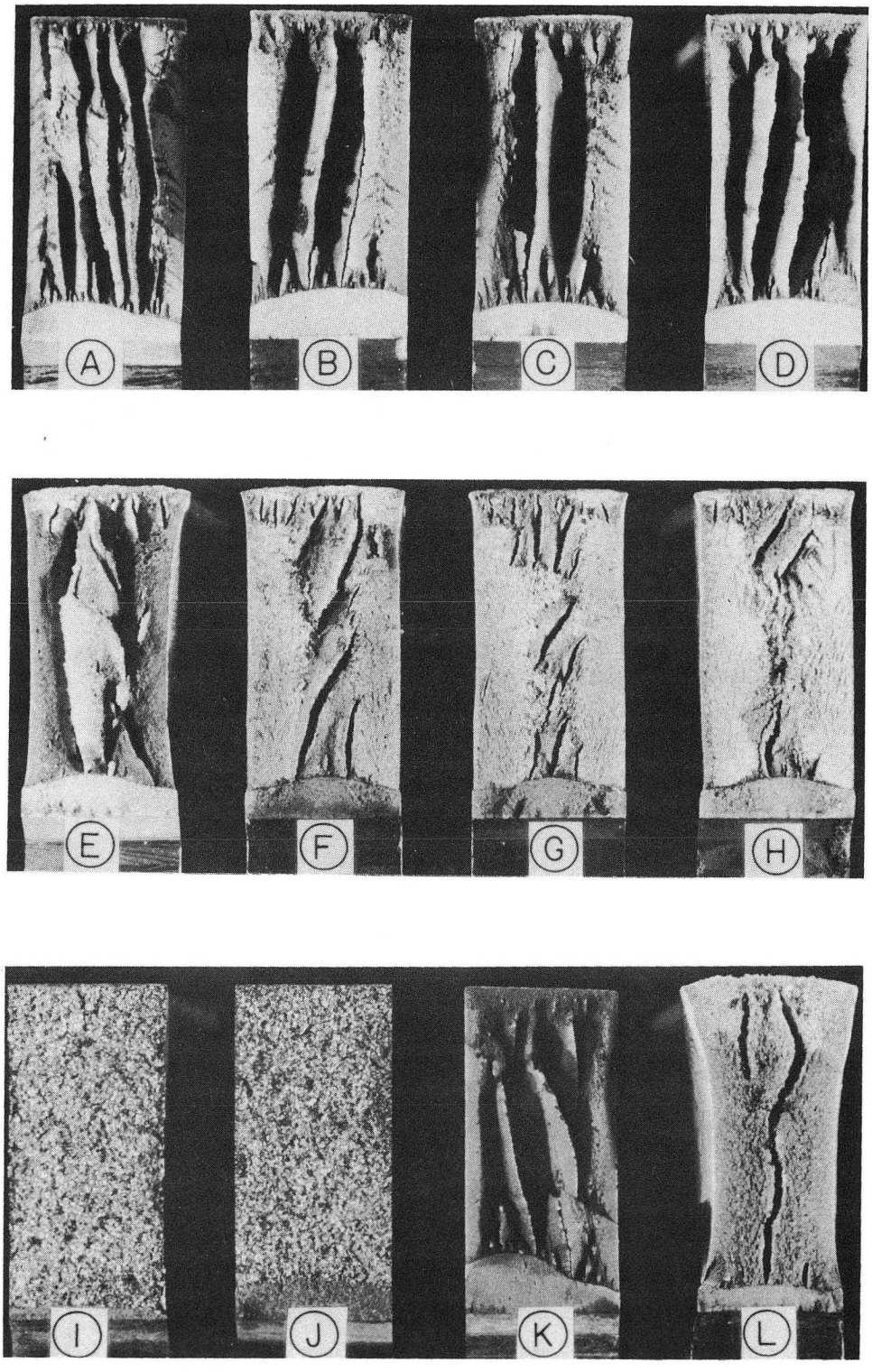

XBB713-921

Figure 8

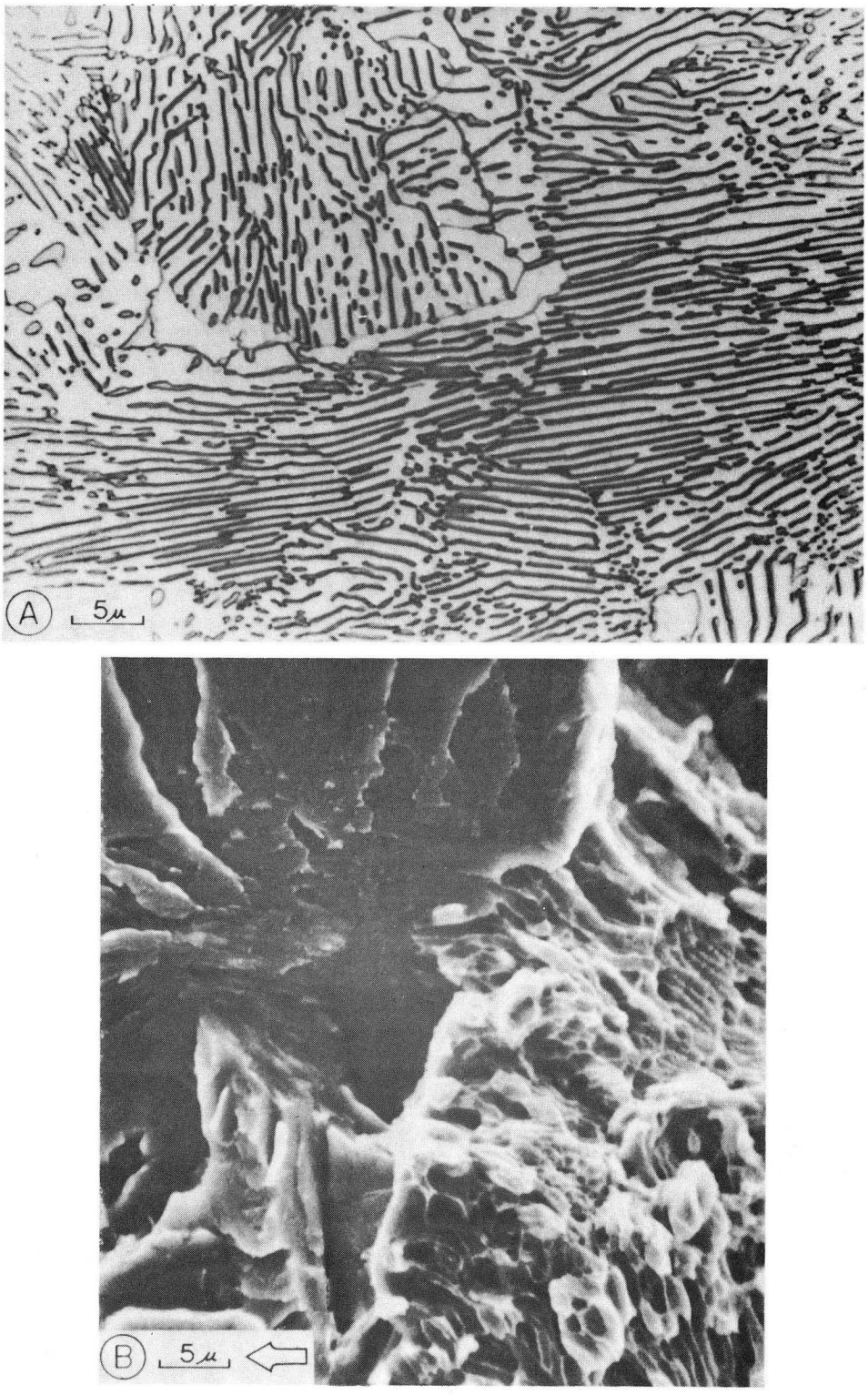

XBB713-917

Figure 9

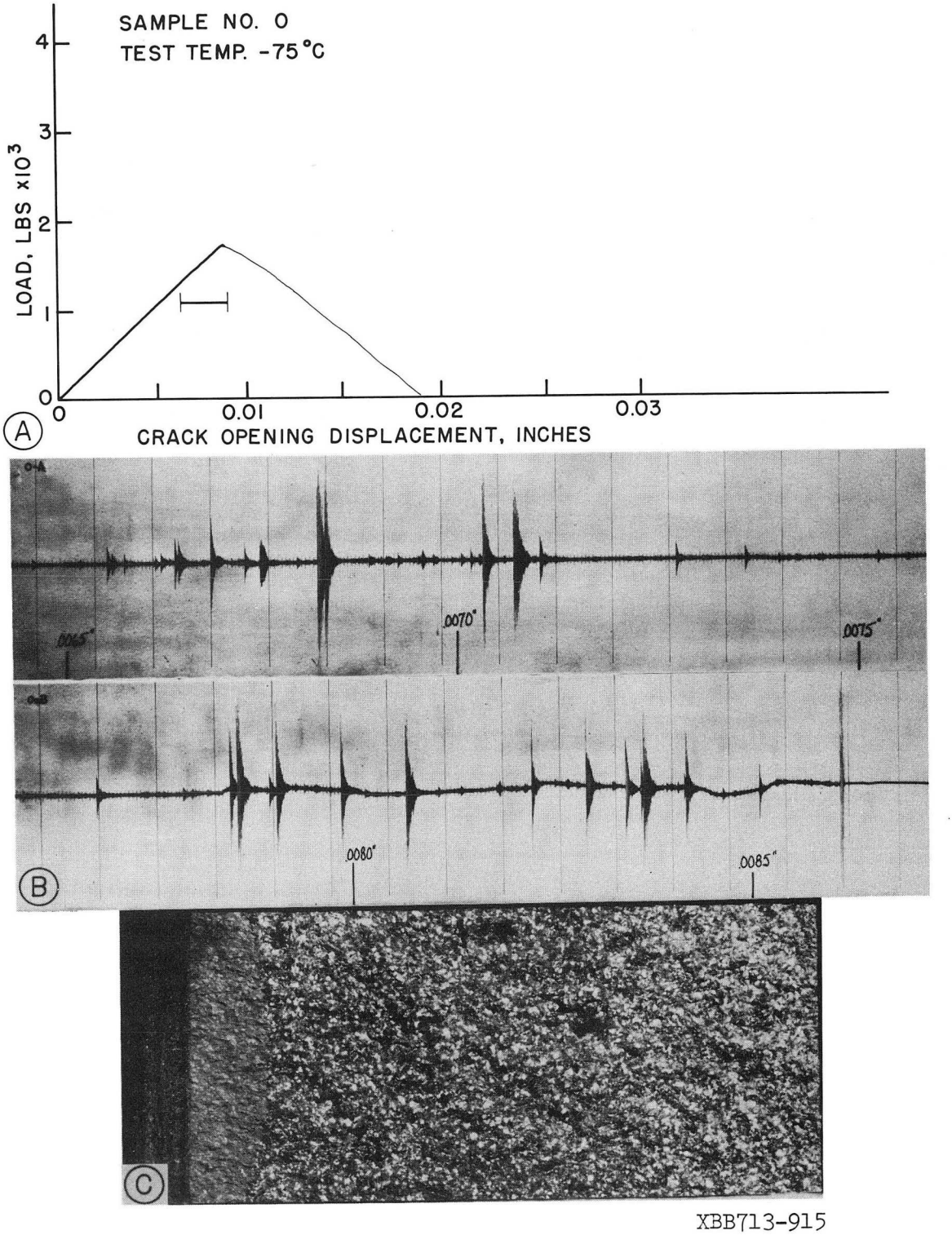

XBB713-915

Figure 10

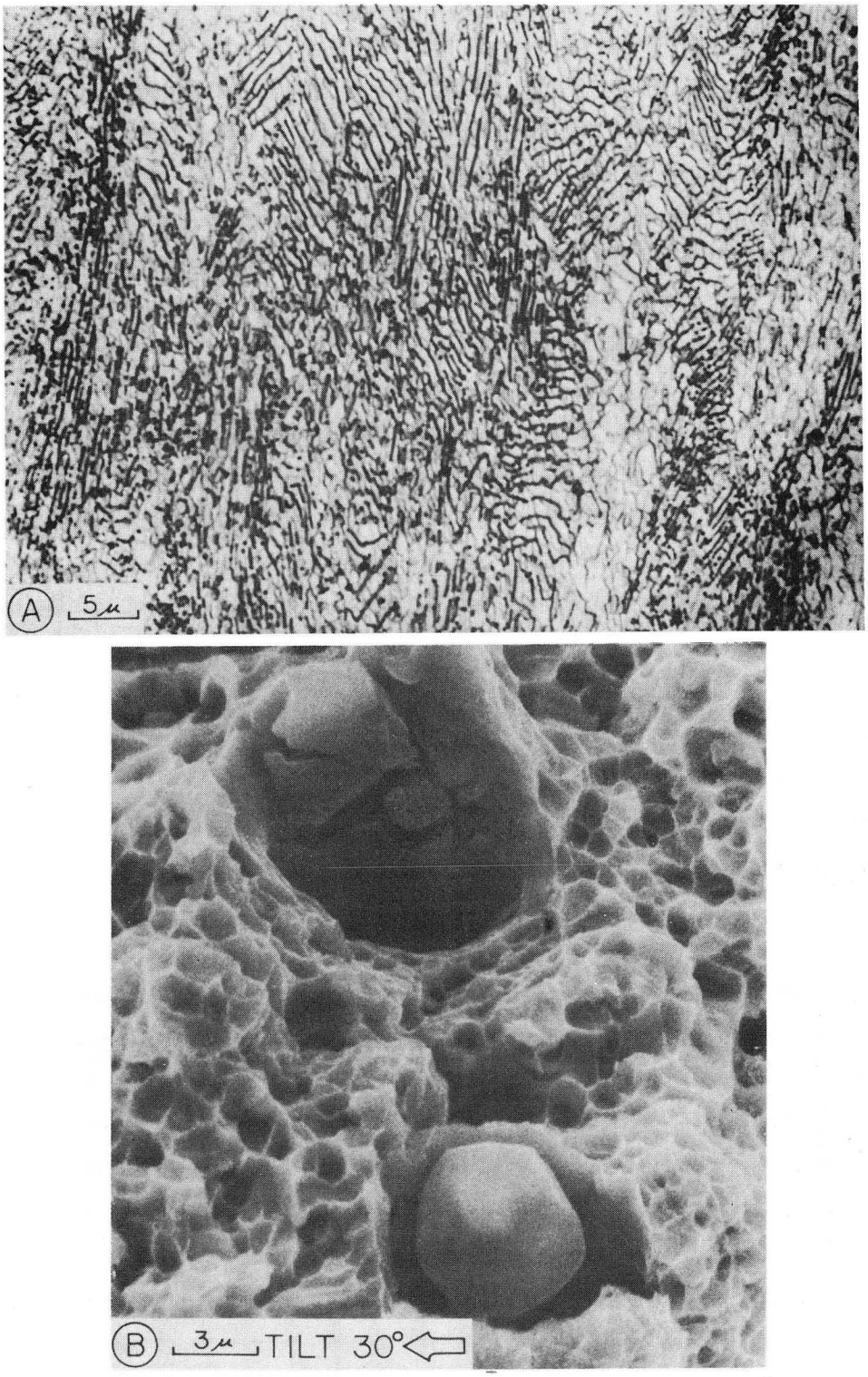

XBB713-916

Figure 11

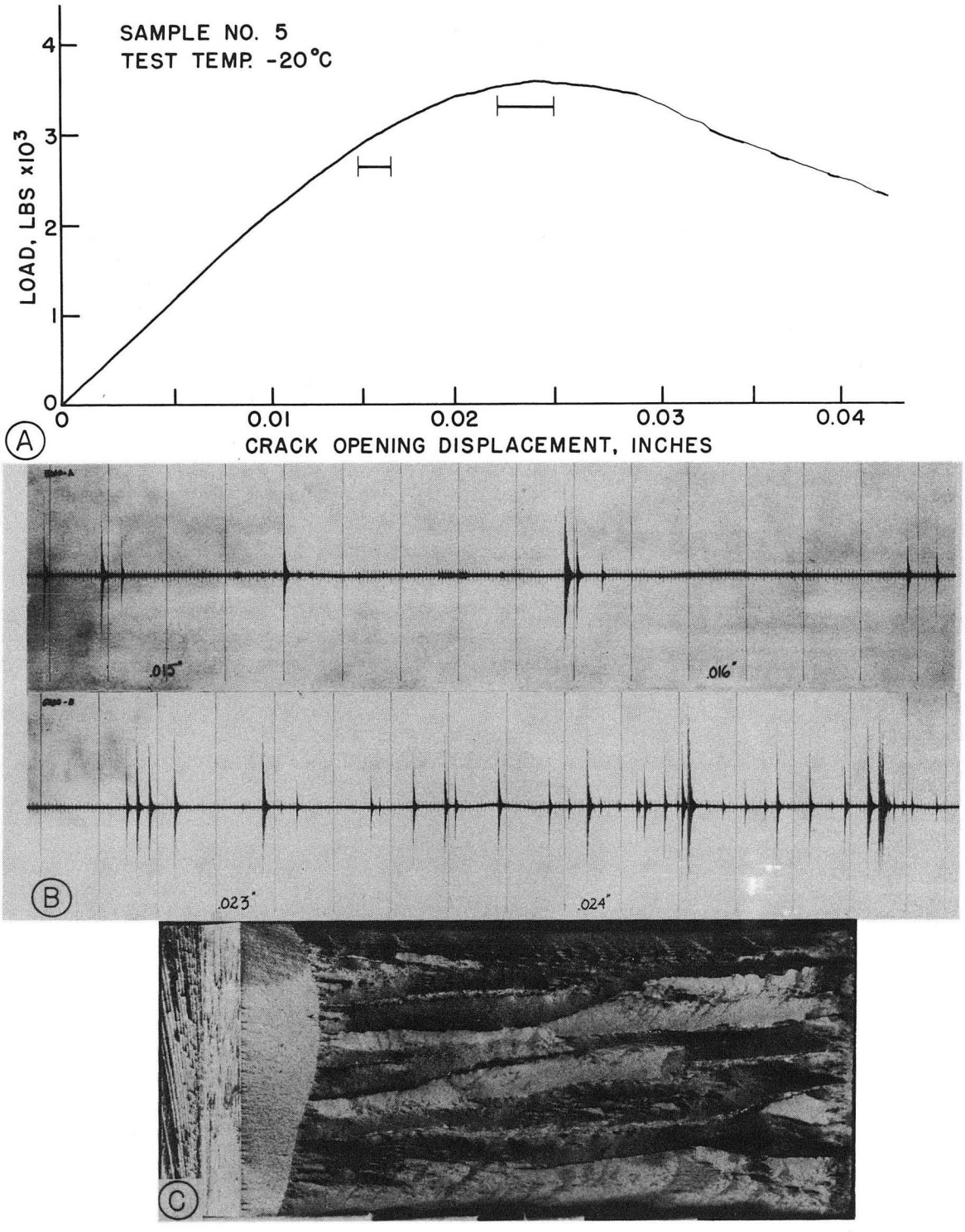

XBB713-914

Figure 12

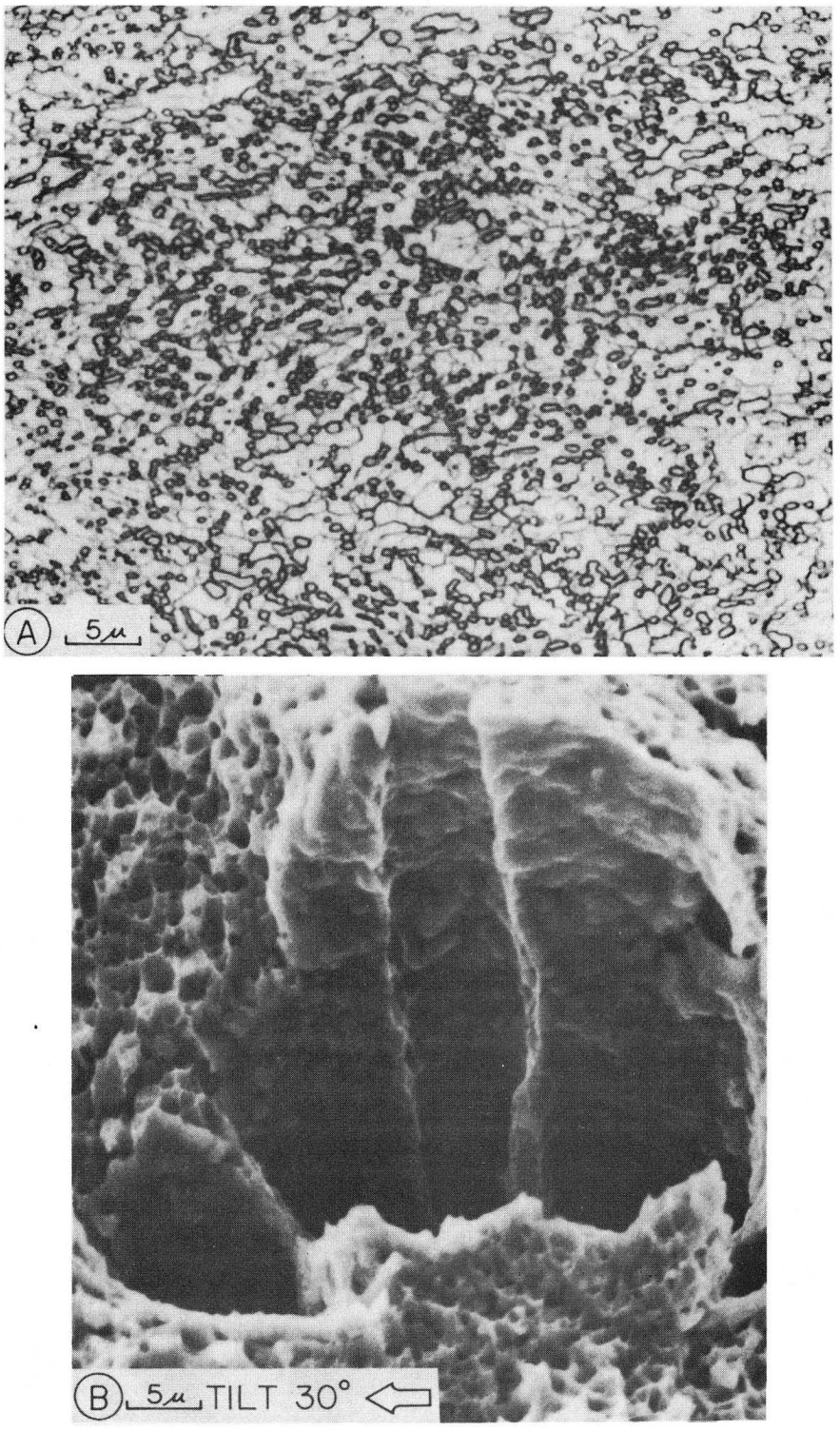

XBB713-919

Figure 13

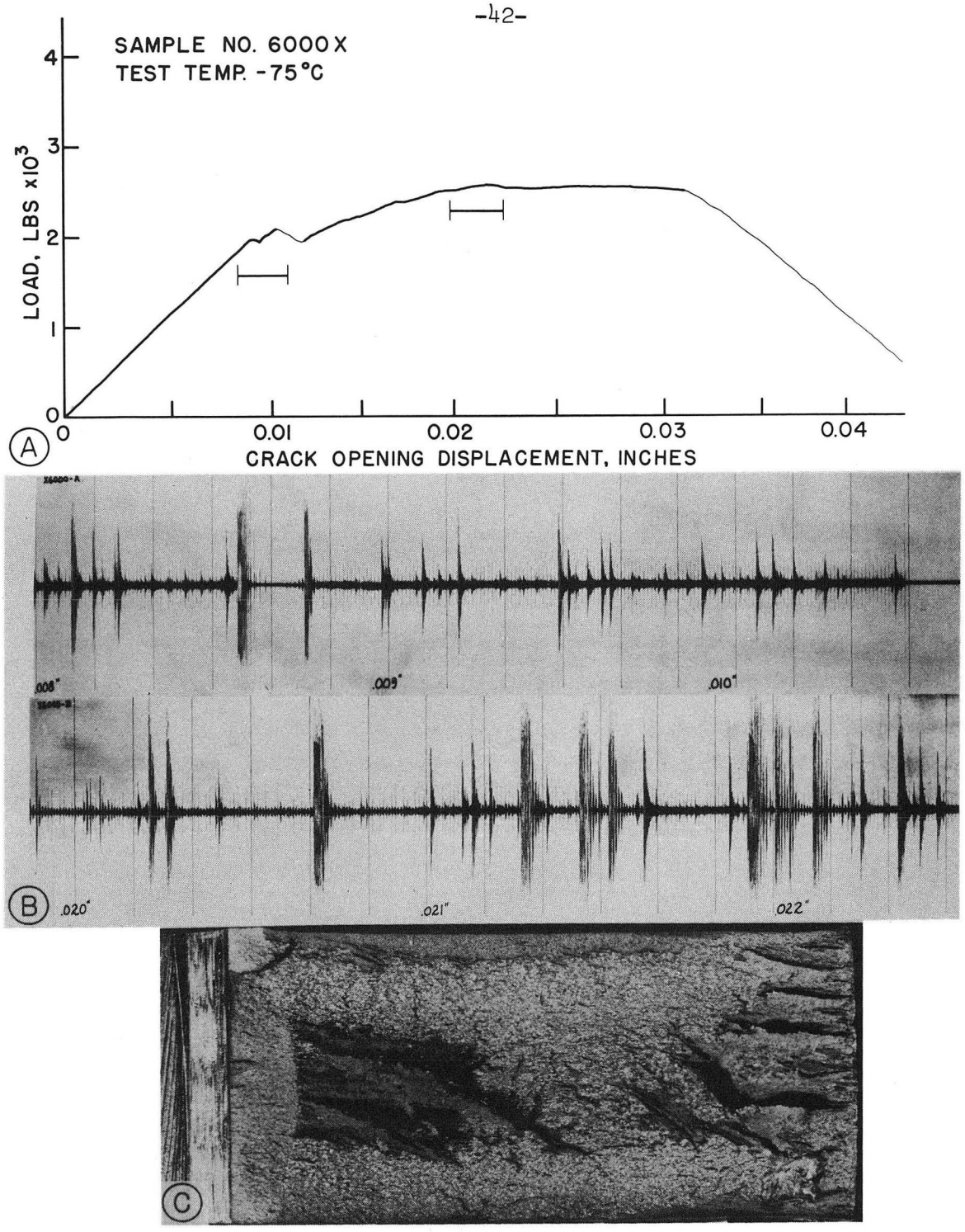

XBB713-910

Figure 14

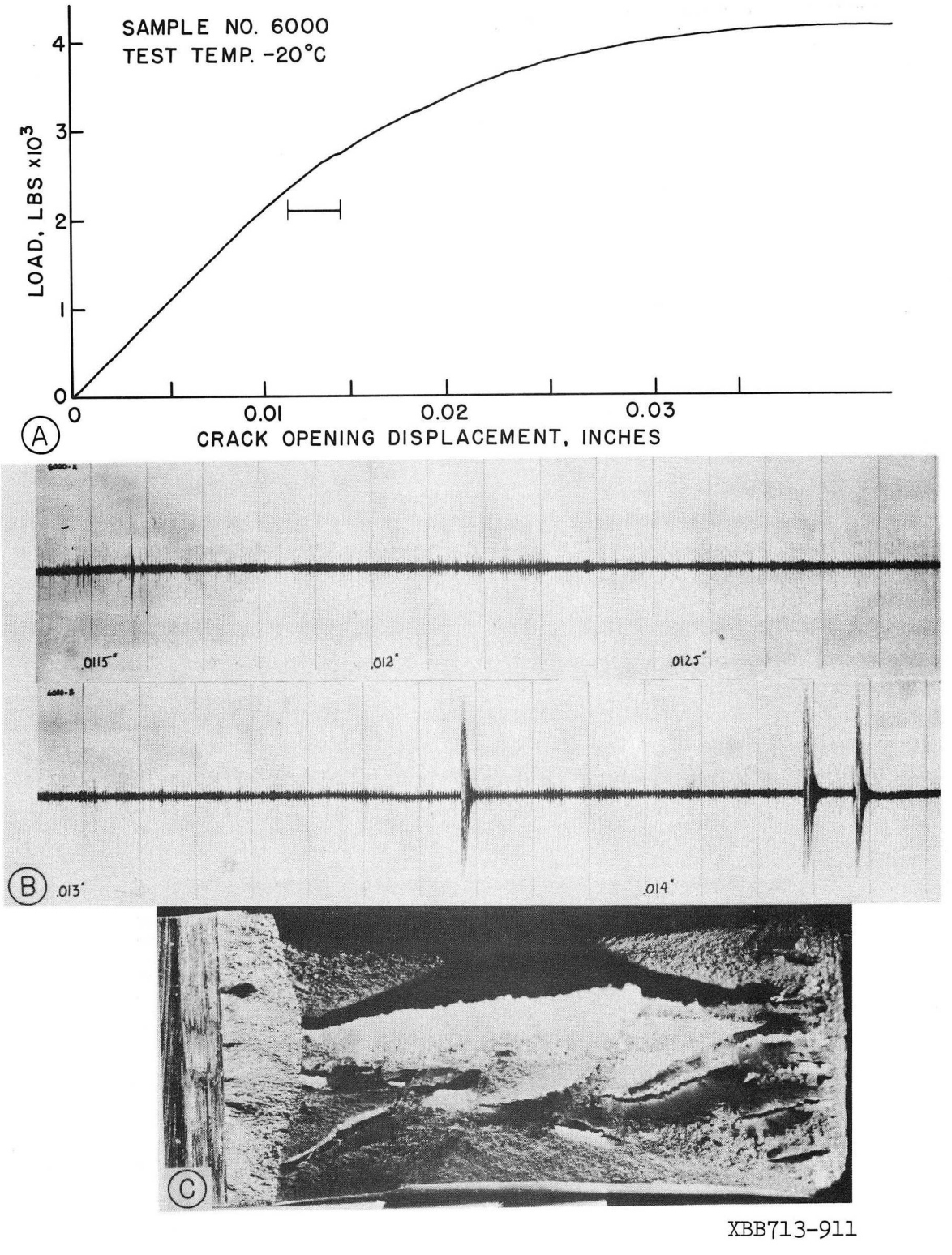

XBB713-911

Figure 15

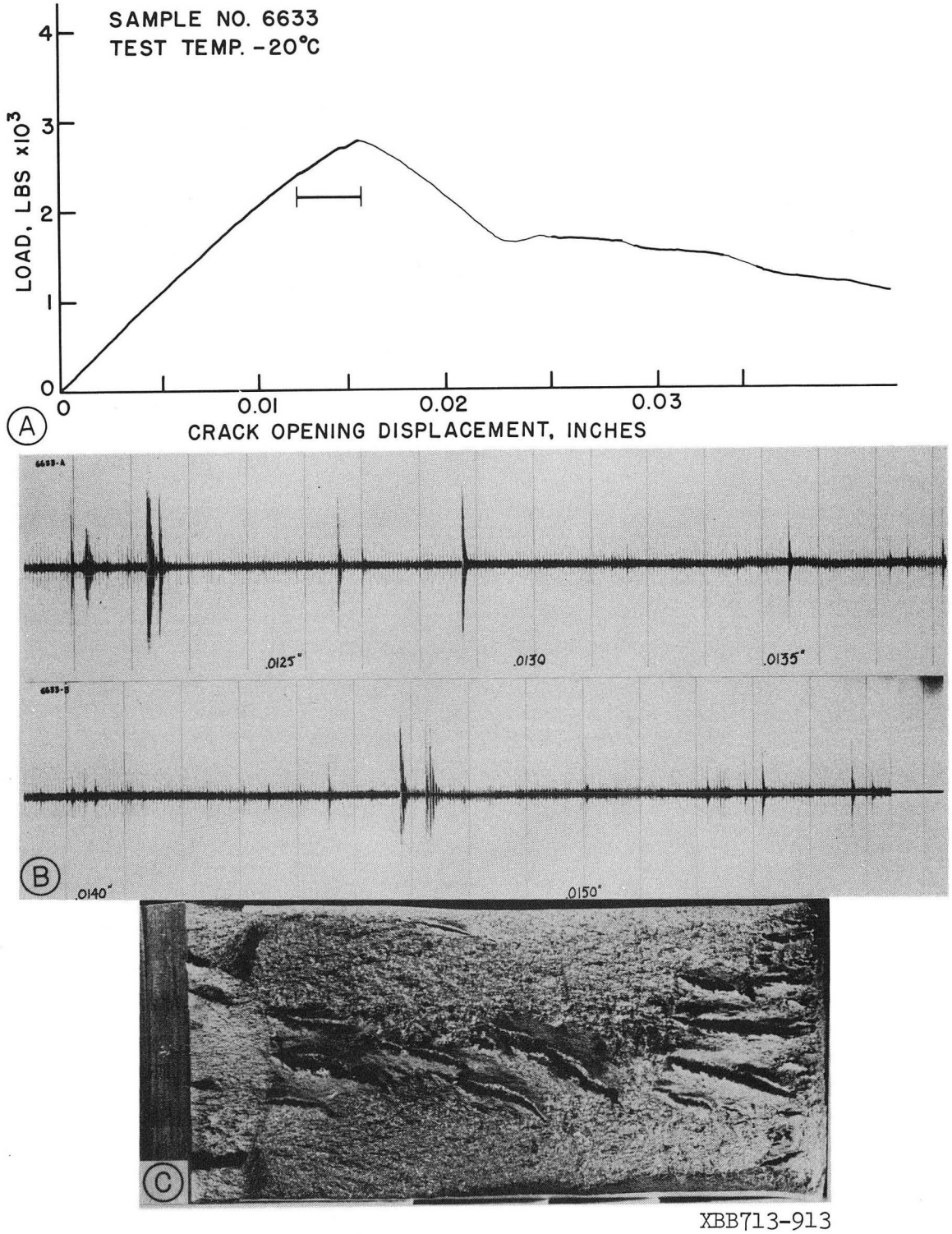

XBB713-913

Figure 16

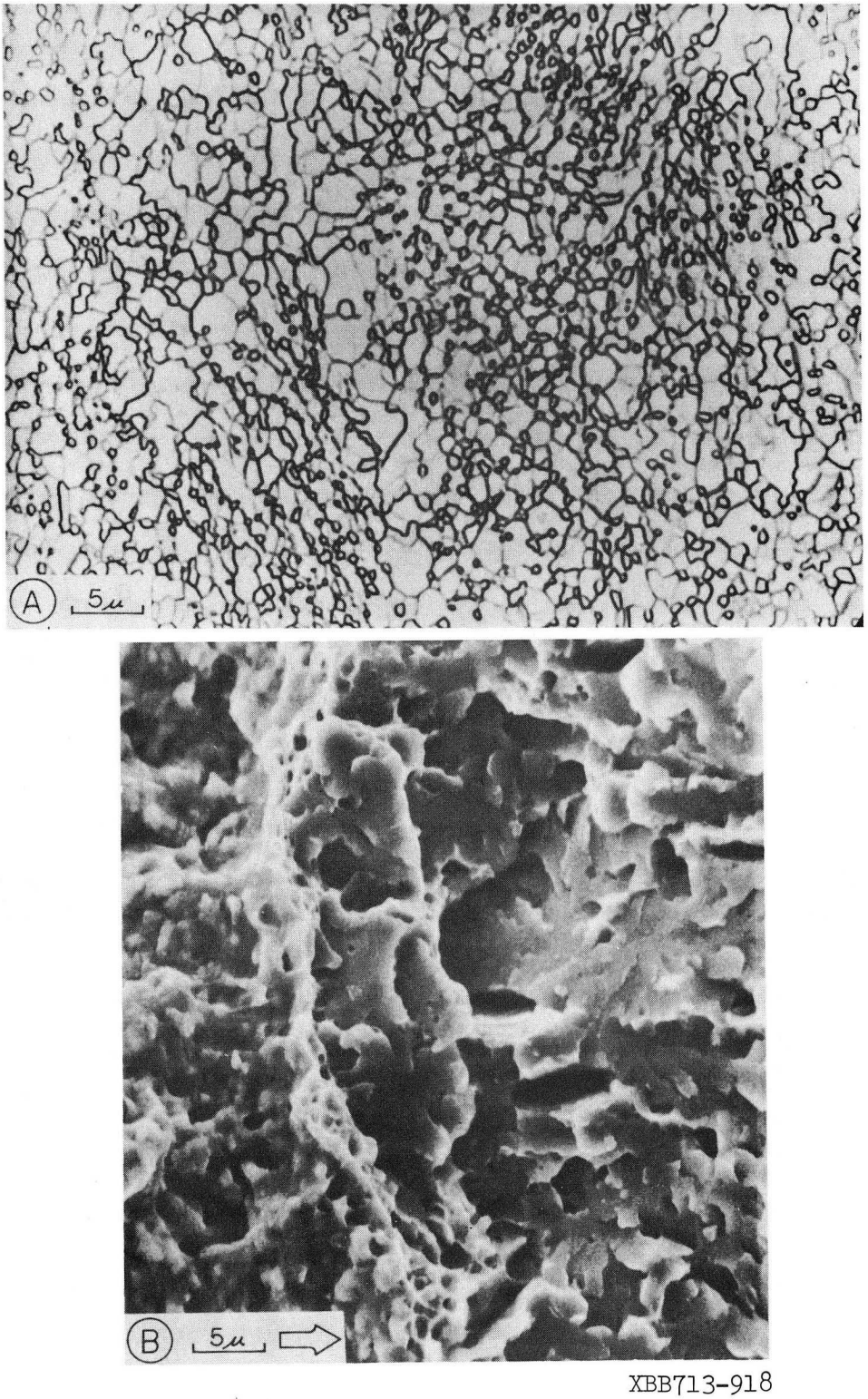

XBB713-918

Figure 17

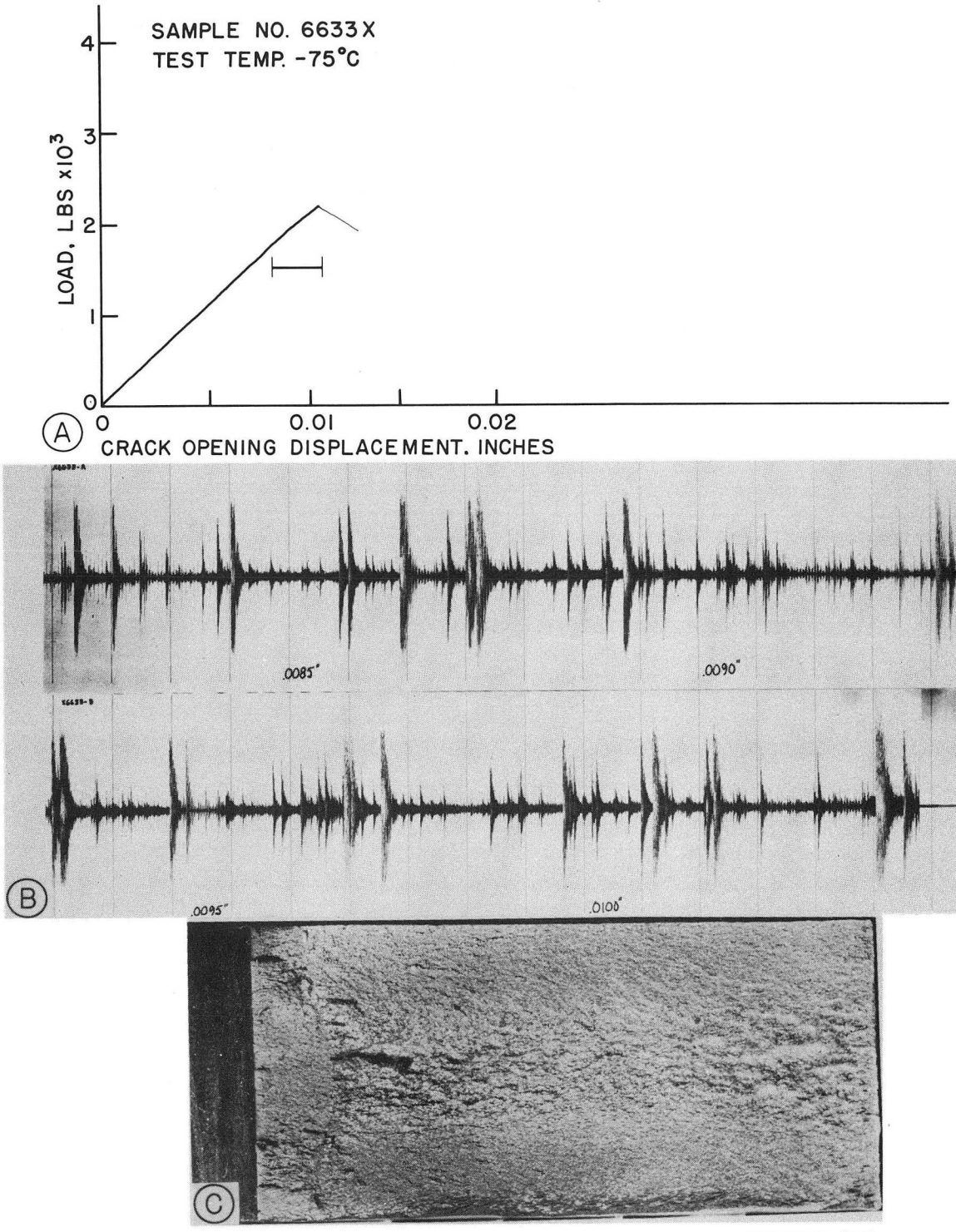
SAMPLE NO. 6633X
TEST TEMP. -75°C
LOAD, LBS x10³
4
3
2
1
0
A
0
0.01
0.02
CRACK OPENING DISPLACEMENT. INCHES
.0085"
.0090"
B
.0095"
.0100"
C
XBB713-912

Figure 18

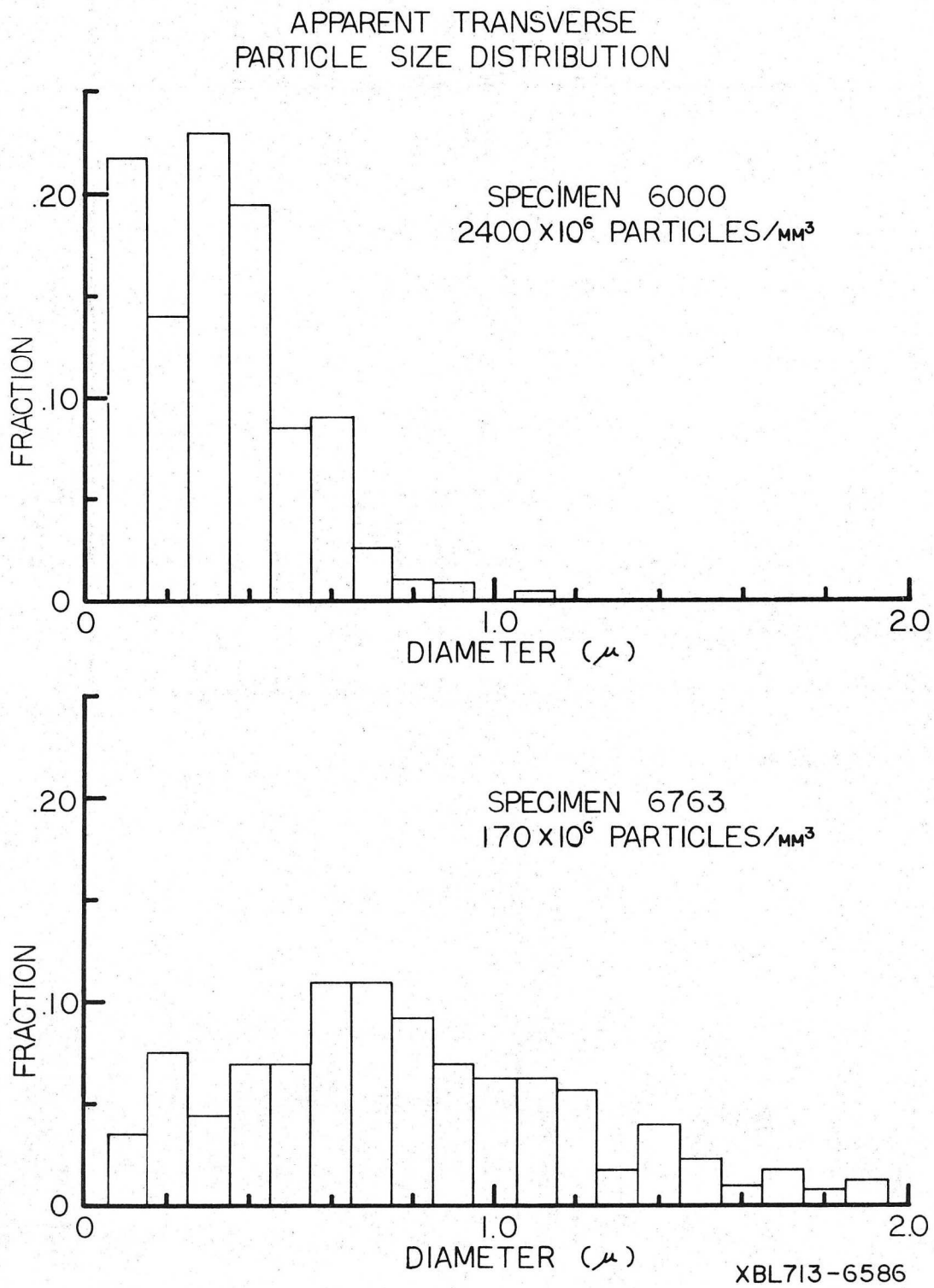
APPARENT TRANSVERSE
PARTICLE SIZE DISTRIBUTION
SPECIMEN 6000
2400 x 10⁶ PARTICLES/MM³
FRACTION
.20
.10
0
0
1.0
2.0
DIAMETER (μ)
SPECIMEN 6763
170 x 10⁶ PARTICLES/MM³
FRACTION
.20
.10
0
0
1.0
2.0
DIAMETER (μ)
XBL713-6586

Figure 19

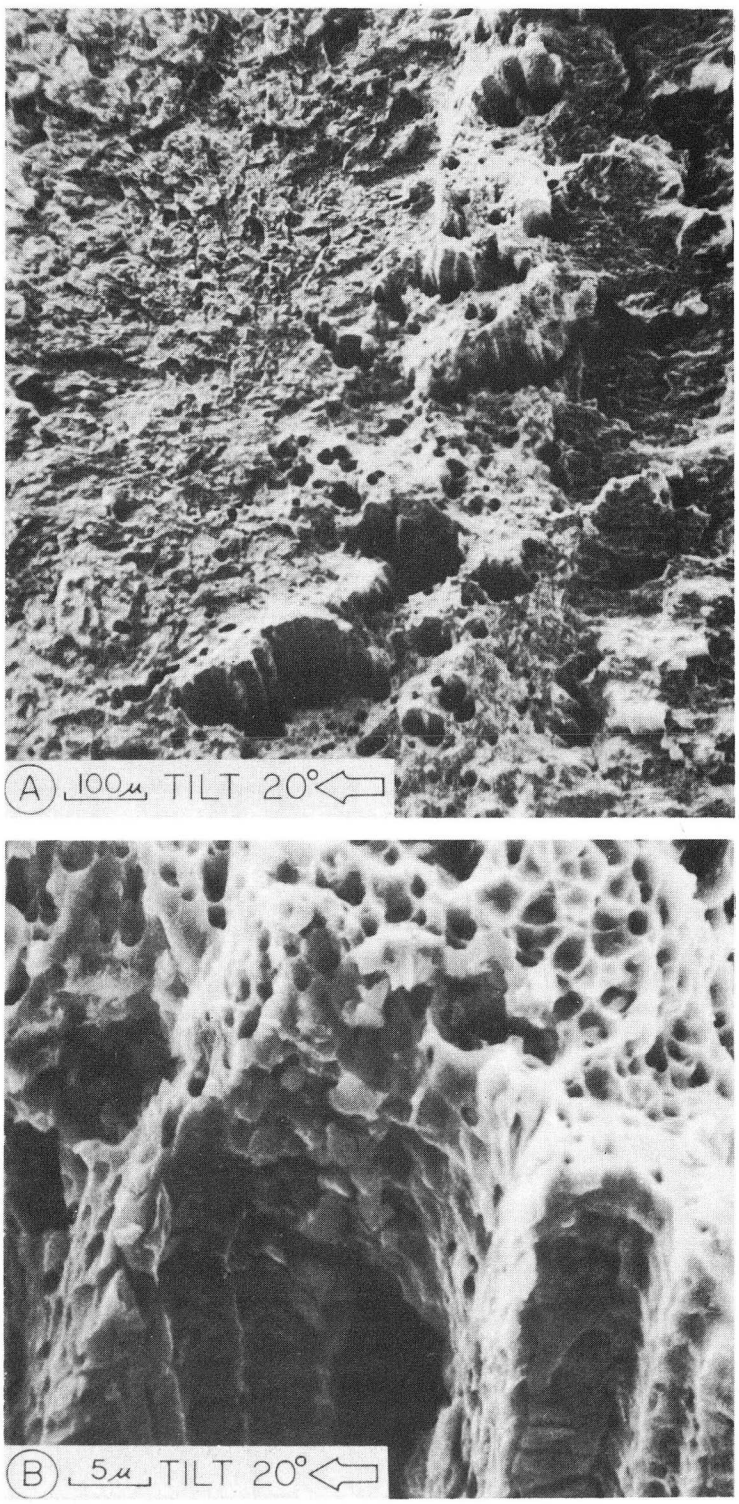

XBB713-920

Figure 20

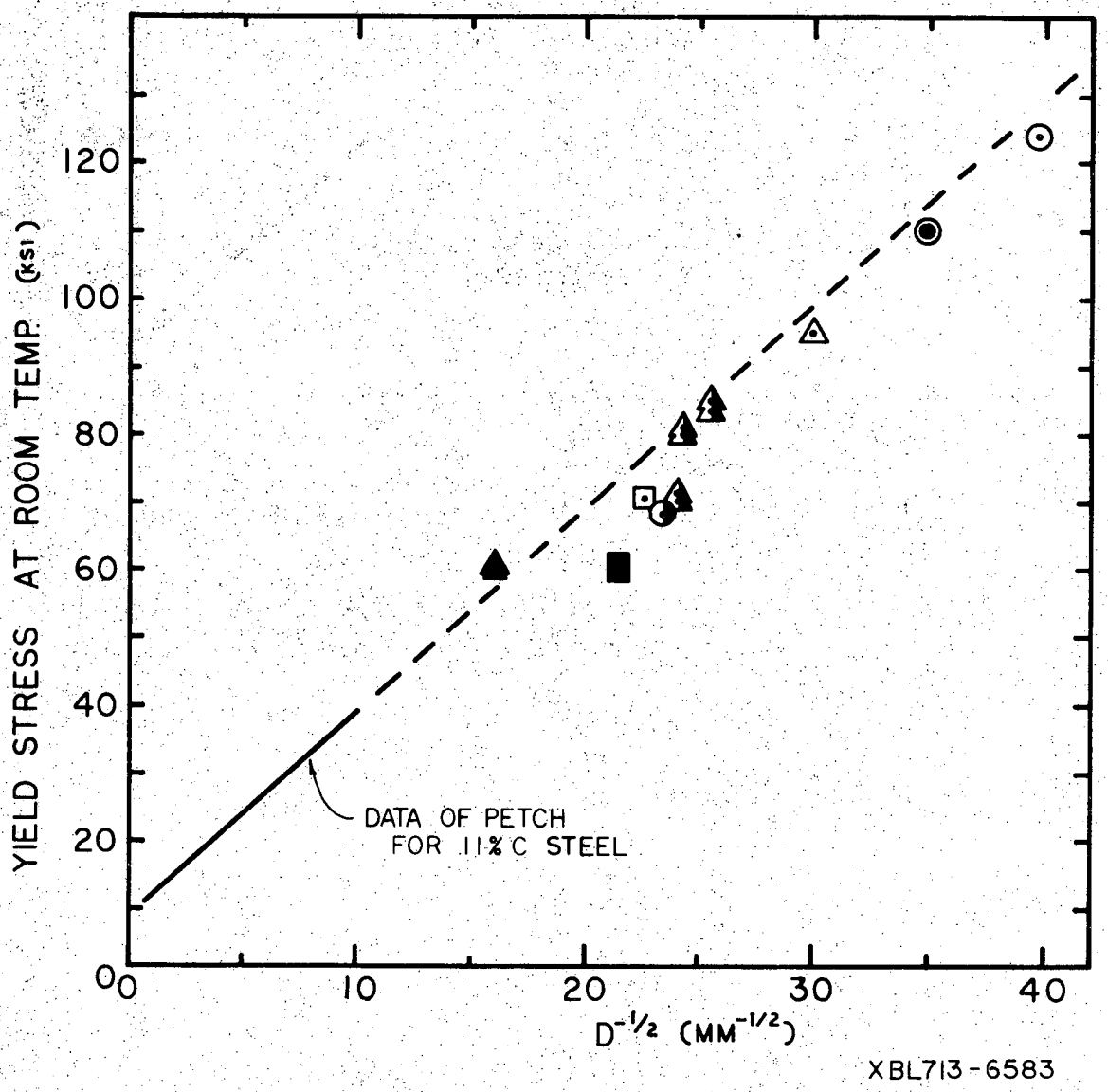
YIELD STRESS AT ROOM TEMP. (ksi)
120
100
80
60
40
20
0
0
10
20
30
40
$D^{-1/2}$ ($MM^{-1/2}$)
DATA OF PETCH
FOR .11% C STEEL
XBL713-6583

Figure 21

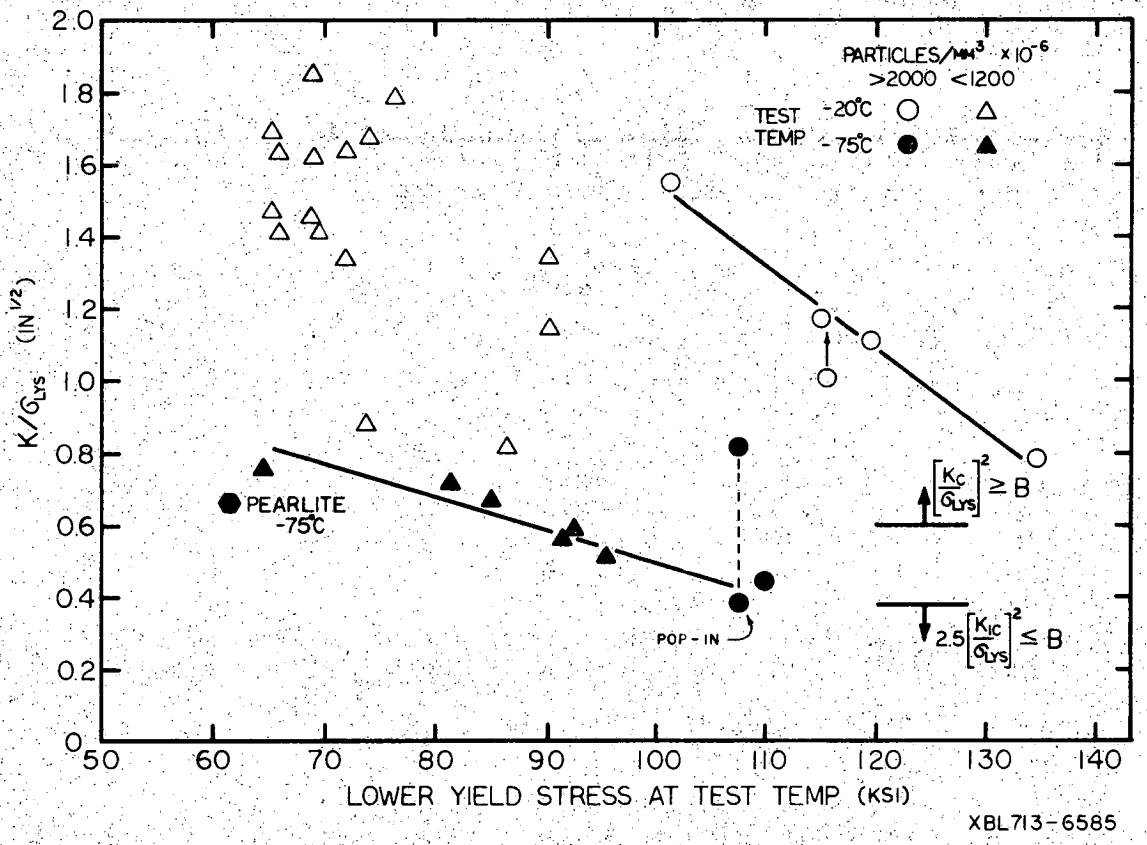
PARTICLES/MM³ x 10⁻⁶
>2000 <1200
TEST TEMP -20°C
-75°C
PEARLITE -75°C
POP-IN
$\left[\frac{K_C}{\sigma_{LYS}}\right]^2 \geq B$
$2.5\left[\frac{K_{IC}}{\sigma_{LYS}}\right]^2 \leq B$
K/σLYS (IN^1/2)
LOWER YIELD STRESS AT TEST TEMP (KSI)
XBL713-6585

Figure 22

TECHNICAL INFORMATION DIVISION
LAWRENCE RADIATION LABORATORY
UNIVERSITY OF CALIFORNIA
BERKELEY, CALIFORNIA 94720